Viral gene therapy approaches for CRB1 retinal disease
Boon, N.

Citation

Boon, N. (2023, November 2). *Viral gene therapy approaches for CRB1 retinal disease*. Retrieved from https://hdl.handle.net/1887/3655975

Chapter 4

AAV-Mediated Gene Augmentation Therapy of *CRB1* Patient-Derived Retinal Organoids Restores the Histological and Transcriptional Retinal Phenotype

N. Boon, X. Lu, C. A. Andriessen, I. Moustakas, T. M. Buck, C. Freund, C. H. Arendzen, S. Böhringer, C.J.F. Boon, H. Mei, and J. Wijnholds
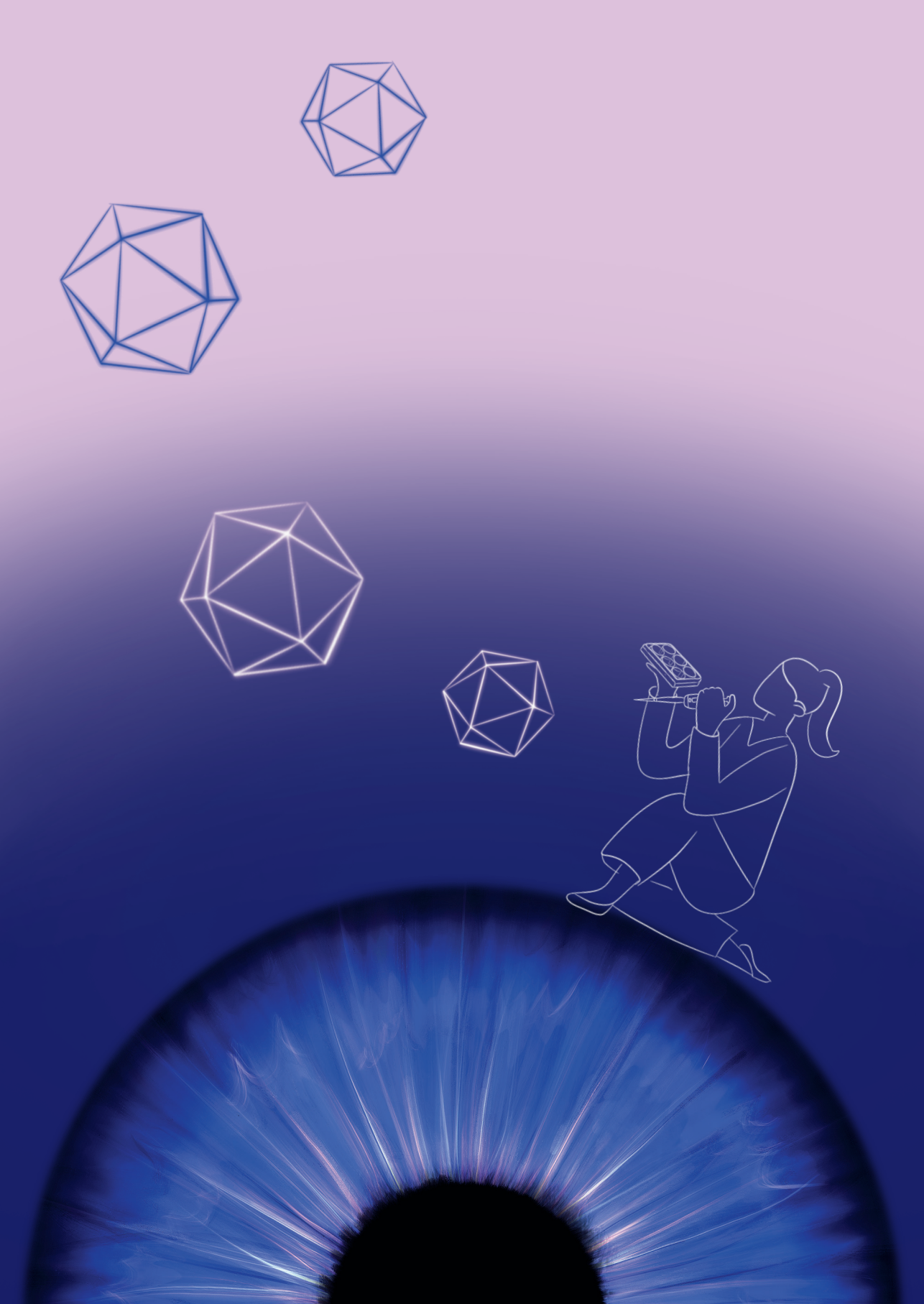
Abstract

Retinitis pigmentosa (RP) and Leber congenital amaurosis are inherited retinal dystrophies which can be caused by mutations in the Crumbs homologue 1 (*CRB1*) gene. CRB1 is required for organizing apical-basal polarity and adhesion between photoreceptors and Müller glial cells. *CRB1* patient-derived induced pluripotent stem cells were differentiated into *CRB1* retinal organoids that showed diminished expression of variant CRB1 protein observed by immunohistochemical analysis. Single cell RNA-sequencing revealed impact on, among others, the endosomal pathway and cell adhesion and migration in CRB1 patient-derived retinal organoids compared to isogenic controls. Adeno-associated viral (AAV) vector-mediated h*CRB2* or h*CRB1* gene augmentation in Müller glial and photoreceptor cells partially restored the histological phenotype and transcriptomic profile of *CRB1* patient-derived retinal organoids. Altogether, we show proof-of-concept that AAV.h*CRB1* or AAV.h*CRB2* treatment improved the phenotype of *CRB1* patient-derived retinal organoids, providing essential information for future gene therapy approaches for patients with mutations in the *CRB1* gene.

Introduction

Retinitis pigmentosa (RP) and Leber congenital amaurosis (LCA) are inherited retinal dystrophies caused by mutations in, among others, the Crumbs homologue 1 (*CRB1*) gene [1–3]. Canonical CRB1 is a large transmembrane protein consisting of a short 37 amino acid intracellular domain containing a protein 4.1, ezrin, radixin, moesin (FERM) and a conserved glutamic acid-arginine-leucine-isoleucine (ERLI) PDZ binding motif, a single transmembrane domain, a large extracellular domain with multiple epidermal growth factor (EGF) and laminin-A globular like domains [1,4,5]. Recently, a short non-canonical alternatively spliced form of CRB1, *CRB1-B*, has been described containing substantial extracellular domain overlap but with distinct amino terminus and lacking the carboxyl terminal transmembrane and intracellular domains [6]. In mammals, canonical CRB1 is a member of the Crumbs family together with CRB2 and CRB3A. The canonical CRB complex is formed by interaction with protein

associated with Lin Seven 1 (PALS1), also known as membrane-associated guanylate kinase p55 subfamily member 5 (MPP5), which binds to the conserved C-terminal PDZ domain of CRB [7–9]. Binding of PALS1 can lead to the recruitment of Multiple PDZ domain protein 1 (MUPP1) or the InaD-like protein (INADL/PATJ) to the apical membrane [7]. This CRB complex is evolutionary conserved and is important for maintaining cell adhesion and regulating apical-basal polarity [10].

So far, no treatment possibilities are available for patients with RP or LCA caused by mutations in *CRB1*. Gene augmentation therapies using adeno-associated viral vectors (AAV) are of emerging interest for retinal dystrophies because of the recent FDA approval of an AAV-mediated gene therapy approach for RP and LCA patients with mutations in the *RPE65* gene [11]. AAVs are the leading platform for gene delivery because of their low toxicity, limited integration into the host genome, and because different AAV capsids display distinct cell tropisms. Their major disadvantage is the limited packaging capacity; inverted terminal repeats, cDNAs and regulatory sequences bigger than 4.9 kb often do not fit in a single AAV capsid. Unfortunately, the full-length cytomegalovirus (CMV) ubiquitous promotor and h*CRB1* cDNA exceeds this packaging limit. However, substantial expression levels of canonical hCRB1 protein in mouse mutant *Crb1* retina were observed using an AAV with codon optimized h*CRB1* cDNA linked to a minimal CMV promoter [12]. This AAV.CMVmin.h*CRB1* was deleterious upon intravitreal injection in Crb1 mouse models [13]. As an alternative approach, *CRB* family member *CRB2* was used to restore retinal function and vision in *Crb* mice [13,14], showing the potential of AAV.h*CRB2* gene augmentation therapy for patients with mutations in the *CRB1* gene.

There are several mouse models described with mutations in the *Crb1* and/or *Crb2* gene mimicking the RP or LCA phenotype [8,15–21]. However, immuno-electron microscopy identified the subcellular localization of CRB1 and CRB2 proteins to be different in mouse and human models. In mice, Crb2 is present in photoreceptor cells and Müller glial cells (MGC) at the subapical region (SAR) of the outer limiting membrane (OLM) while Crb1 is solely present in MGC at the SAR [22]. In contrast, in human fetal retina and human induced pluripotent stem cell (hiPSC)-derived retinal

organoids both CRB1 and CRB2 are observed at the SAR in photoreceptors and MGC [23]. This discrepancy suggests the importance of using human-derived models for gene therapy approaches.

Here, we describe the phenotype of differentiation day 210 (DD210) and DD230 patient-derived retinal organoids harboring *CRB1* missense mutations compared to isogenic controls in more detail using immunohistochemical analysis and single-cell RNA sequencing. Next, the effect of AAV-mediated h*CRB1* or h*CRB2* gene augmentation therapy was analyzed on *CRB1* patient-derived and isogenic control retinal organoids. A partially improved retinal phenotype of *CRB1* patient-derived retinal organoids was observed, providing crucial data for future gene therapy approaches for patients with mutations in the *CRB1* gene.

Results

Reduced number of photoreceptor nuclei and thinner outer nuclear layer (ONL) in DD210 CRB1 patient-derived retinal organoids compared to isogenic controls

Retinal organoids were differentiated from hiPSC lines derived from three *CRB1* RP patients: (1) LUMC0116iCRB with c.3122T>C p.(Met1041Thr) homozygote missense mutations (here abbreviated as: P116), (2) LUMC0117iCRB with 2983G>T p.(Glu995*) and c.1892A>G, p.(Tyr631Cys) mutations (P117), and (3) LUMC0128iCRB with c.2843G>A p.(Cys948Tyr) and c.3122T>C p.(Met1041Thr) missense mutations (P128) [23]. Isogenic controls for P116 and P128 were generated by CRISPR/Cas9; (1) ISO-02 P116 with a homozygous correction, (2) ISO-03 P116 with a heterozygous correction, and (3) ISO-P128 a heterozygous correction of Cys948Tyr (Supplemental Table 1). Genomic stability of all iPSC lines was tested by a digital PCR test of the copy number variants (CNV) of 90% of the most recurrent abnormalities in hiPSC [24]. No aberrant CNV were observed in the hiPSC lines used in this study (Supplemental Figure 1A).

Previous research has shown that *CRB1* patient-derived retinal organoids at DD180 show disruptions at the OLM and photoreceptor nuclei protruding above the OLM [23]. Here, we analyzed the phenotype of the CRB1 patient-derived retinal organoids at a later timepoint (DD210) and compared those to the isogenic controls. By light microscopy, no visible difference was observed in cultured retinal organoids comparing *CRB1* patient with the isogenic controls at DD210: all contained a translucent region at the outside of the organoid (the ONL) with inner and/or outer-segment-like structures around the retinal organoid Figure 1A, Supplemental Figure 1B).

Immunohistochemistry of rod photoreceptor marker rhodopsin and MGC marker SOX9 at DD210 revealed the presence of rod photoreceptors and SOX9 positive MGCs for both patient and isogenic controls (Figure 1B, 1C, Supplemental Figure 1C, 1D).

When analyzing the phenotype in more detail, a moderate but statistically significant decrease in the number of photoreceptor nuclei and ONL thickness was observed in *CRB1* patient-derived retinal organoids compared to isogenic controls (Figure 1D). In contrast to *CRB1* patient-derived retinal organoids at DD180 [23], no statistically significant difference in the number of photoreceptor nuclei above the OLM was detected at DD210 (Figure 1D). In addition, no statistically significant differences were observed for the total retinal thickness and the inner nuclear layer (INL) thickness of the retinal organoids (Supplemental Figure 1F).

Missense mutations in CRB1 result in reduced levels of variant CRB1 protein in CRB1 patient-derived retinal organoids

Immunohistochemistry analysis of all three *CRB1* patient-derived retinal organoids at DD210 shows a diminished CRB1 staining at the OLM compared to the isogenic control (Supplemental Figure 1E, 1E). Similar strongly diminished levels of variant CRB1 in *CRB1* patient-derived retinal organoids compared to the isogenic control were observed at DD180 (Supplemental Figure 1G). While CRB2 and CRB complex members MUPP1 and PALS1 remain at the OLM in both isogenic and *CRB1* patient-derived organoids (Figure 1E, 1F, Supplemental Figure 1F).
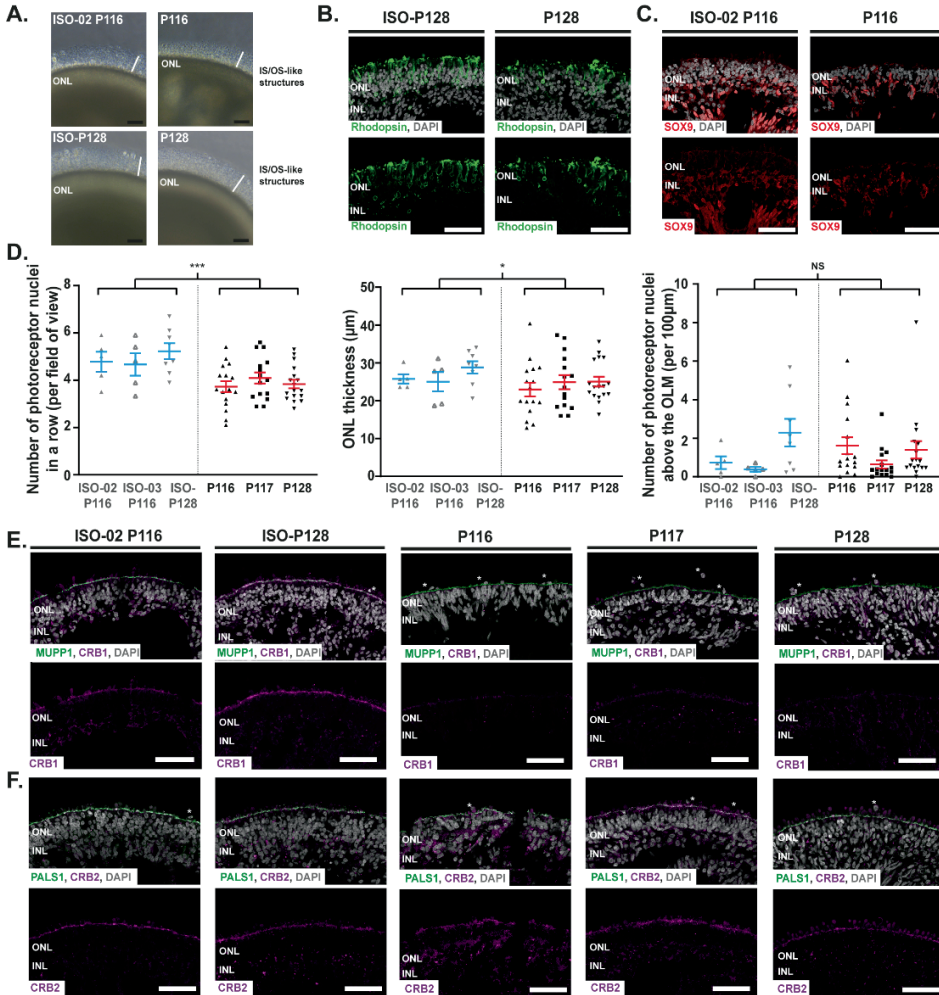
Figure 1. *CRB1* patient and isogenic control phenotypic analysis at DD210. (A) Representative brightfield images of ISO-02 P116, P116, ISO-P128, and P128 cultured organoids. (B) Representative immunohistochemical images of rhodopsin (green) in ISO-P128 and P128. (C) Representative immunohistochemical images of SOX9 (red) in ISO-P116 and P116. (D) Quantitative analysis of number of photoreceptor nuclei in a row per field of view ($p = 0.000$), ONL thickness per field of view ($p = 0.049$), and number of photoreceptor nuclei above the OLM per 100μm ($p = 0.651$) in *CRB1* patient-derived and isogenic control retinal organoids. (E) Immunohistochemical images of CRB1 (red) and MUPP1 (green) in *CRB1* patient-derived retinal organoids with two appropriate isogenic controls. (F) Immunohistochemical images of CRB2 (red) and PALS1 (green) in *CRB1* patient-derived retinal organoids with two appropriate isogenic controls. Each datapoint in the graph represent individual organoids, of which an average has been taken of 3-6 representative images. The

standard error of mean (SEM) is derived from these averages. Number of individual organoids per condition and differentiation round: P116 n = 16, P117 n = 15, P128 n = 17 from four independent organoid batches, ISO-P128 n = 8 from three independent organoid batches, ISO-02 P116 n = 5 and ISO-03 P116 n = 5 from two independent organoid batches. Scalebar = 50µm, statical analysis: generalized linear mixed models with $p < 0.05$ (*), $p < 0.01$ (**), and $p < 0.001$ (***). Related to Supplemental Figure 1.

Missense mutations in CRB1 do not affect the levels of CRB1 or CRB2 RNA transcripts in CRB1 patient-derived retinal organoids

Next, we used single cell RNA sequencing (scRNA-seq) to identify differences in RNA transcripts and gene ontology pathways between DD230 *CRB1* patient-derived retinal organoids and isogenic controls. Transcriptionally similar cells were grouped and visualized (R package *Seurat*), revealing distinct clusters with differentially expressed marker genes (Supplemental Table 3). These identified expressed genes per cluster were compared to known retinal marker genes to classify clusters. Major retinal cell types could be visualized on a UMAP plot, such as MGC, photoreceptor cells (both rods and cones), bipolar cells, amacrine cells, horizontal cells, ganglion cells and retinal pigment epithelium (RPE) (Figure 2A). In addition, some of the clusters consisted of astrocytes and transitory cells (Figure 2A), and tissue that is generally attached to the retinal organoid was observed and classified as stromal cells (Figure 2A, Supplemental 2C). The expression of key cell-type specific markers of all clusters are shown in a feature plot and heatmap (Figure 2B, Supplemental Figure 2A). Interestingly, two rod photoreceptor cell subtypes can be distinguished. Upon further analysis, cluster rods I was identified to be composed of more mature cells with significantly higher transcript expression levels of *NR2E3*, *PDE6B* and *RHO* in comparison to cluster rods II (Supplemental Figure 2B) [25].

We confirmed that all the major retinal cell clusters were equally present in both P128 and ISO-P128 (Figure 2C) and P116 and ISO-P116 (Supplemental Figure 3A). Expression levels of both *CRB1* and *CRB2* were predominantly observed in MGC and photoreceptor cells. When analyzing *CRB1* expression levels in MGC and photoreceptor cells in more detail, no statistically significant differences were observed between P128 and ISO-P128 (Figure 2D) nor between P116 and ISO-P116

(Supplemental Figure 3B). Rods I and rods II were combined into a general "rods" cluster, since no statistically significant differences were observed in the individual clusters (data not shown). Moreover, the sequence of *CRB1-B*, an alternative transcript of CRB1 containing distinct 5' and 3' ends, was added to the pre-built reference and was not detected in our DD230 retinal organoids (Supplemental Figure 2D). While *CRB1-B* transcripts were detected in adult human retina cDNA, the levels of *CRB1-B* transcripts were below detection level by reverse transcription quantitative real-time PCR (RT-qPCR) on DD210 retinal organoids (data not shown; Supplemental experimental procedures). In addition, no statistically significant difference was observed for the *CRB2* expression level (Figure 2E, Supplemental Figure 3C), nor for canonical CRB core complex members *PALS1*, *MUPP1*, *PATJ* (Figure 2F, Supplemental Figure 3D) or for FERM proteins *MSN*, *EZR*, or *EPB41L5* (Supplemental Figure 2E).

Gene profiling shows disruptions in the endosomal system in MGC and rods

Differential gene expression analysis followed by Gene Ontology (GO) term analysis comparing *CRB1* patient and isogenic control retinal organoids was performed. Analysis of P128 and ISO-P128 specifically in the MGCs, where most *CRB1* is expressed, revealed five groups of similar gene ontology terms containing differentially expressed genes deregulated in the patient-derived retinal organoids. The first gene ontology group is involved in the endosomal system, including extracellular exosomes, vesicles, endomembrane system, and early endosomes (Figure 2G). The second group is involved in the maintenance of location in the cell, cell motility, proliferation and cell-cell adhesion, the third group revealed differences in proteins containing various binding domains such as ferric iron and fatty acid, while the fourth group is involved in cell death (Figure 2G). Finally, the last one is a mixed group with pathways such as iron ion transport and post-translational protein phosphorylation (Figure 2G). In addition, as the *CRB1* transcript is also present in photoreceptor cells, differentially expressed markers and subsequent gene ontology terms were analyzed in rods (combination of rods I and rods II) and cones. In rods, gene ontology terms involved in the endosomal system were observed to be differentially expressed (Figure 2H). In
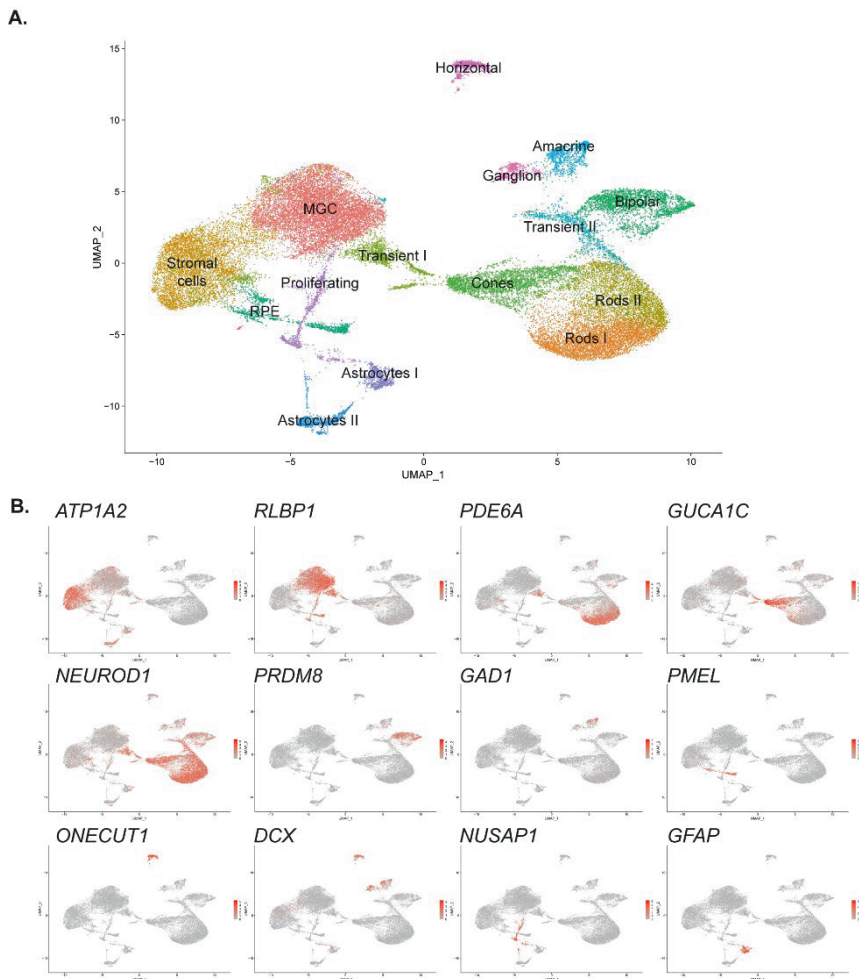
Figure 2 (A-B): scRNA-seq analysis comparing ISO-P128 with P128 shows disruptions in the endosomal system in Müller glial cells and rods. (A) UMAP plot of observed clusters and (B) expression plots of top markers indicating the distinct clusters. Number of independent organoids used: ISO-P128 $n = 6$, and P128 $n = 6$ from one differentiation round equally divided into three separate sequencing rounds. Related to Supplemental Figure 2 and 3.

addition, markers associated with the activation of the phototransduction cascade were detected (Figure 2H). No statistically significant differential expressed markers were observed in cone photoreceptor cells (data not shown).
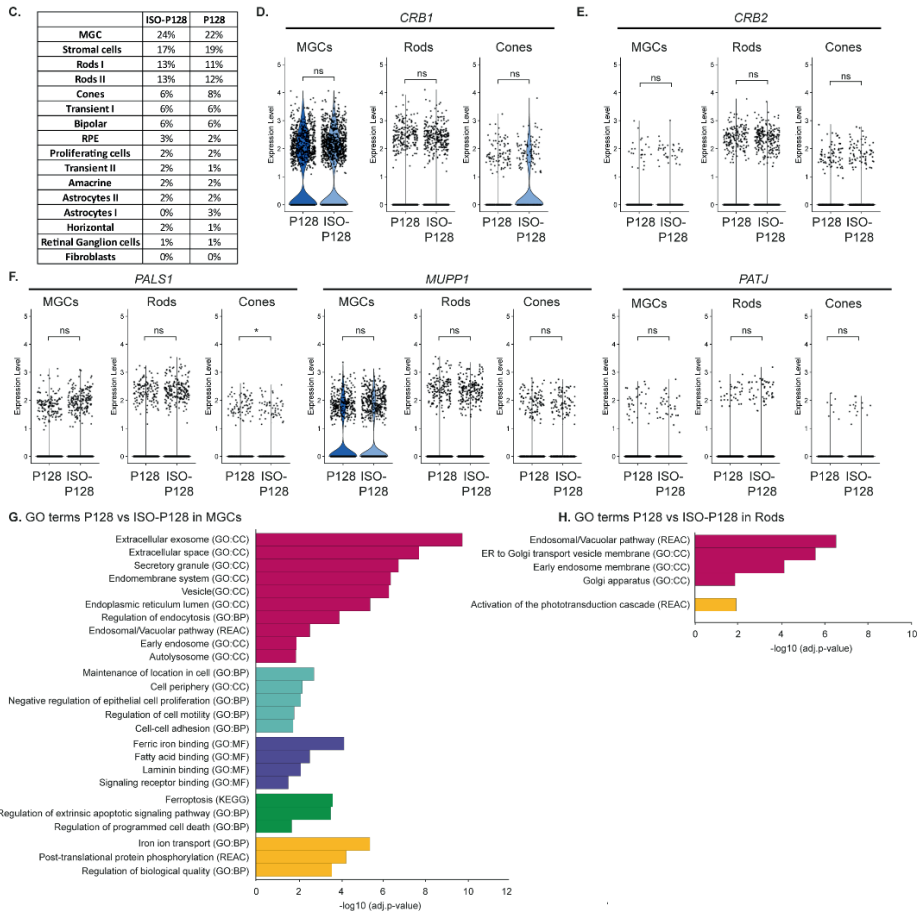
Figure 2 (C-H): scRNA-seq analysis comparing ISO-P128 with P128 shows disruptions in the endosomal system in Müller glial cells and rods (C) Table showing that all retinal cell types are present in both lines. (D) Violin plots of *CRB1* transcript levels specifically in MGCs ($p = 0.93$), rods ($p = 0.84$) and cones ($p = 0.72$). (E) Violin plots of *CRB2* transcript levels specifically in MGCs ($p = 0.43$), rods ($p = 0.18$) and cones ($p = 0.85$). (F) Violin plots of canonical core CRB complex members *PALS1*, *MUPP1*, and *PATJ* transcript levels in MGCs ($p = 0.32$; $p = 0.51$; $p = 0.73$, respectively), rods ($p = 0.97$; $p = 0.18$; $p = 0.63$), and cones ($p = 0.025$; $p = 0.25$; $p = 0.87$). (G, H) Gene ontology (GO) analysis of differentially expressed markers specifically in MGCs (G) and rods (H) clustered in groups with similar terms in the same colour. Number of independent organoids used: ISO-P128 $n = 6$, and P128 $n = 6$ from one differentiation round equally divided into three separate sequencing rounds. Related to Supplemental Figure 2 and 3.

Such an analysis was also performed comparing P116 with ISO-P116, where gene ontology terms associated with the endosomal system were differentially expressed in

rod photoreceptor cells (Supplemental Figure 3E). No statistically significant gene ontology terms were observed in MGC, explained by the low number of differentially expressed genes and the low number of cells sequenced in this cluster. Altogether, this data shows aberrations in the endosomal system between *CRB1* patient-derived retinal organoids compared to their isogenic controls.

Serotype AAV5.CMV.GFP is more efficient than AAV2.CMV.GFP in transducing Müller glial cells at DD120

CRB1 protein is localized at the OLM in human and non-human primate MGC and photoreceptors [17,23], and higher levels of *CRB1* transcript are found in MGC than in photoreceptors (Figure 2D). For AAV-mediated gene therapy approaches in *CRB1* patient-derived retinal organoids it is therefore essential to transduce sufficient number of MGC in addition to photoreceptors. Therefore, we identified which cells are transduced using specific viral capsids and titers at DD120. Control retinal organoids were transduced with $1x10^{10}$gc, $6,6x10^{10}$gc or $10x10^{10}$gc AAV2/5.CMV.*GFP* (AAV5.CMV.*GFP*) or AAV2/2.CMV.*GFP* (AAV2.CMV.*GFP*) and analyzed using immunohistochemistry after three weeks in culture.

A significant dose-dependent increase of GFP-positive cells was observed when control organoids were treated with AAV5.CMV.*GFP* or AAV2.CMV.*GFP* at DD120 (Supplemental Figure 3F, 3G). The AAV treated retinal organoids were quantified for number of GFP-positive cells in the ONL, the INL, and GFP-positive cells in the INL which were also SOX9 positive (marking MGCs). AAV2.CMV.*GFP* transduced more photoreceptor cells in the ONL than AAV5.CMV.*GFP* (Figure 3C). However, AAV5.CMV.*GFP* transduced more cells in the INL than AAV2.CMV.*GFP* (Figure 3D). More specifically, more SOX9-positive MGCs were transduced with AAV5.CMV.*GFP* than with AAV2.CMV.*GFP* (Figure 3E). Co-staining with photoreceptor markers (OTX2 and recoverin) and MGC markers (CRALBP and SOX9) confirmed the transduction of both cell types in AAV2.CMV.*GFP* as well as AAV5.CMV.*GFP* transduced organoids at DD120 (Figure 3F, G). Moreover, a 10x

magnification of a retinal organoid treated with $10x10^{10}$gc AAV5.CMV.*GFP* at DD120 showed that most of the retinal organoid was transduced in our experiment (Figure 3H).

Because AAV5 transduced more MGCs than AAV2, treatment with AAV5 at DD120 was used for further AAV.h*CRB* gene augmentation therapy with an intermediate dose of $3,3x10^{10}$gc.

AAV-mediated hCRB gene augmentation therapy partially restores the histological phenotype of CRB1 patient-derived retinal organoids

After defining the AAV.GFP tropism, preclinical gene therapy approaches were performed on *CRB1* patient-derived retinal organoids using AAV5.CMVmin.h*CRB1* or AAV5.CMV.h*CRB2* (here abbreviated as: AAV.h*CRB1* and AAV.h*CRB2*, respectively) at DD120 and analyzed at DD180 or DD210.

Immunohistochemical analysis and subsequent quantification of retinal organoids transduced with AAV.h*CRB1* or AAV.h*CRB2* and analyzed at DD180 show an increased number of photoreceptor nuclei in a row in AAV.*CRB* treated P117 compared to the control (Supplemental Figure 4B). In addition, fewer photoreceptor nuclei protruding above the OLM were observed after AAV.*CRB* treatment of P117 compared to the control organoids (Supplemental Figure 4C). No statistically significant difference was observed for the retinal nor the ONL thickness in both CRB1 patient and control organoids treated with AAV.h*CRB1* or AAV.h*CRB2* (Supplemental Figure 4D, 4E).

In addition, the long-term gene augmentation effect was examined for multiple *CRB1* patient-derived lines, where the organoids were collected and analyzed at DD210. One group of three different *CRB1* patient-derived retinal organoids was treated with solely AAV.h*CRB1* or AAV.h*CRB2* or left untreated, while in the following experiment the *CRB1* patient-derived retinal organoids were treated with AAV.h*CRB1* with AAV.*GFP*, or AAV.h*CRB2* with AAV.*GFP*, or AAV.*GFP* alone. Adding AAV.*GFP* facilitates in defining the regions where the AAV.h*CRB* most likely infected.
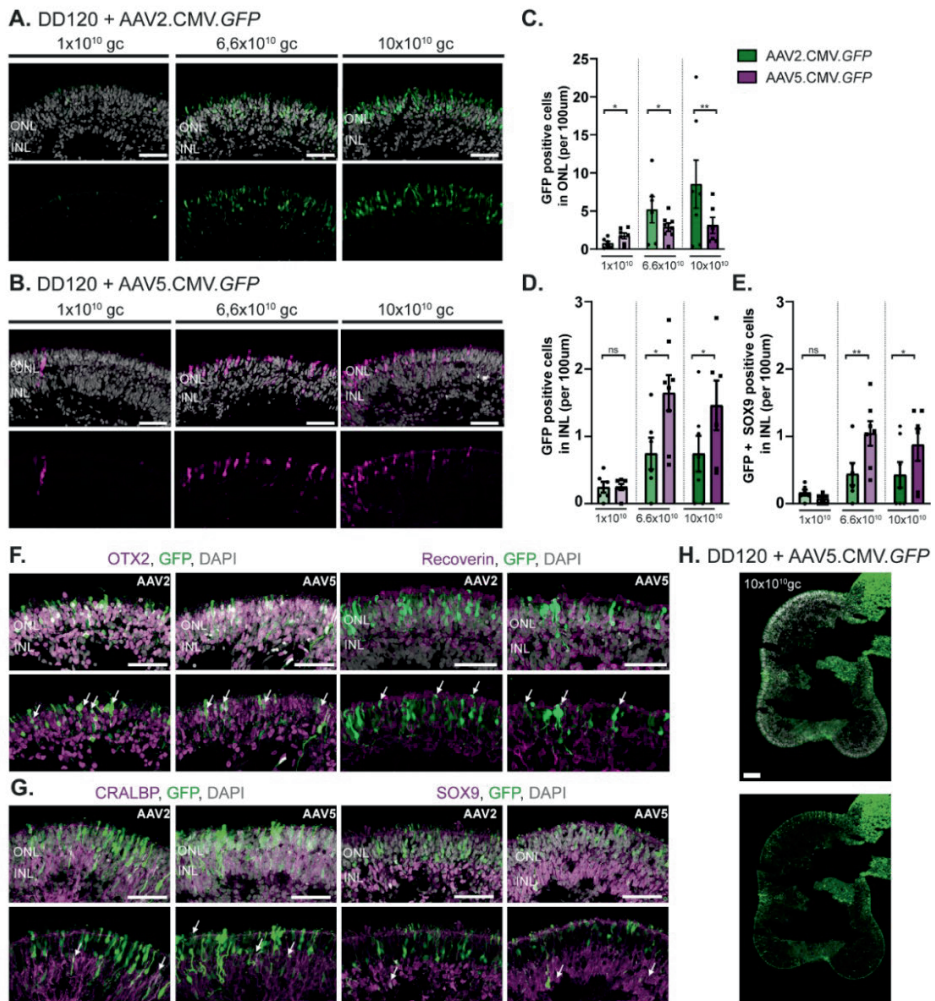
Figure 3: AAV2.CMV.*GFP* and AAV5.CMV.*GFP* transduction of DD120 control retinal organoids. (A,B) Representative immunohistochemical images of (A) AAV2.CMV.*GFP* and (B) AAV5.CMV.*GFP* treated control organoids at DD120 with three different titer concentrations: $1x10^{10}$, $6.6x10^{10}$, and $10x10^{10}$ gc (genome copies). (C, D, E) Quantification of AAV treated retinal organoids with AAV2.CMV.GFP or AAV5.CMV.GFP at the (C) ONL, (D) INL, or (E) GFP positive MGC in the INL. (F, G) Representative immunohistochemical images of photoreceptor cells marker (OTX2 and recoverin) and MGC markers (CRALBP and SOX9) showing colocalization with AAV.*GFP* for both AAV2.CMV.*GFP* and AAV5.CMV.*GFP* treated organoids. (H) Representative 10x magnification immunohistochemical analysis of DD120 control organoid transduced with $10x10^{10}$gc AAV5.CMV.*GFP*. Immunohistochemical images of (F, G, and H) are merged z-stack views, the others are single image views. Scalebar = 50μm. Each datapoint in the graph represent individual organoids, of which an average has been

taken of at least 3 representative images. The standard error of mean (SEM) is derived from these averages. Number of individual organoids per condition: for AAV2.CMV.*GFP* $1x10^{10}$ $n = 5$, $6.6x10^{10}$ $n = 6$, and $10x10^{10}$ $n = 7$, and for AAV5.CMV.*GFP* $1x10^{10}$ $n = 7$, $6.6x10^{10}$ $n = 8$, and $10x10^{10}$ $n = 6$ individual organoids from two independent differentiation rounds. Statical analysis: generalized linear mixed models with $p < 0.05$ (*), $p < 0.01$ (**), and $p < 0.001$ (***). Related to Supplemental Figure 3.

Fluorescent images of organoids in culture co-treated with AAV.*GFP* and AAV.h*CRB* show the presence of GFP positive regions, while no visible differences were observed between treated and untreated organoids using bright field or fluorescent images (Figure 4A). Immunohistochemical staining of CRB1 in AAV.h*CRB1* or CRB2 in AAV.h*CRB2* treated retinal organoids showed proof of recombinant CRB protein localization at the OLM and in the RPE (Figure 4B, 4C, Supplemental Figure 4F, 4G, 4H, 4I). Further immunohistochemical analysis showed a partially improvement in the observed phenotype after AAV.h*CRB1* or AAV.h*CRB2* treatment (Figure 4D, E, F). For quantitative analysis, all three *CRB1* patient-derived retinal organoids with and without concomitant treatment of AAV.*GFP* were pooled. No statistically significant difference was observed in fluorescence intensity of MUPP1 at the OLM in untreated compared to AAV.h*CRB* treated *CRB1* patient-derived retinal organoids (Supplemental Figure 4J). In addition, the expression of another core CRB-complex member, PALS1, is not changed after AAV.h*CRB* treatment (Supplemental Figure 4K).

A statistically significant increased number of photoreceptor nuclei in a row was detected after AAV.h*CRB1* and AAV.h*CRB2* treatment at DD210, while this large difference was not observed in the treated isogenic controls (Figure 4G). Moreover, the ONL thickness (but not the retinal nor the INL thickness) was significantly increased after AAV.h*CRB* treatment of *CRB1* patient-derived retinal organoids (Figure 4H, Supplemental Figure 4L, 4M). Finally, the number of photoreceptor nuclei above the OLM was significantly improved after AAV.h*CRB2* treatment of *CRB1* patient-derived retinal organoids at DD210 (Figure 4I). No statistically significant improvement in the number of photoreceptor nuclei above the OLM was observed after AAV.h*CRB1* treatment of *CRB1* patient-derived retinal organoids nor after AAV.h*CRB1* or AAV.h*CRB2* treatment in the control retinal organoids (Figure 4I).
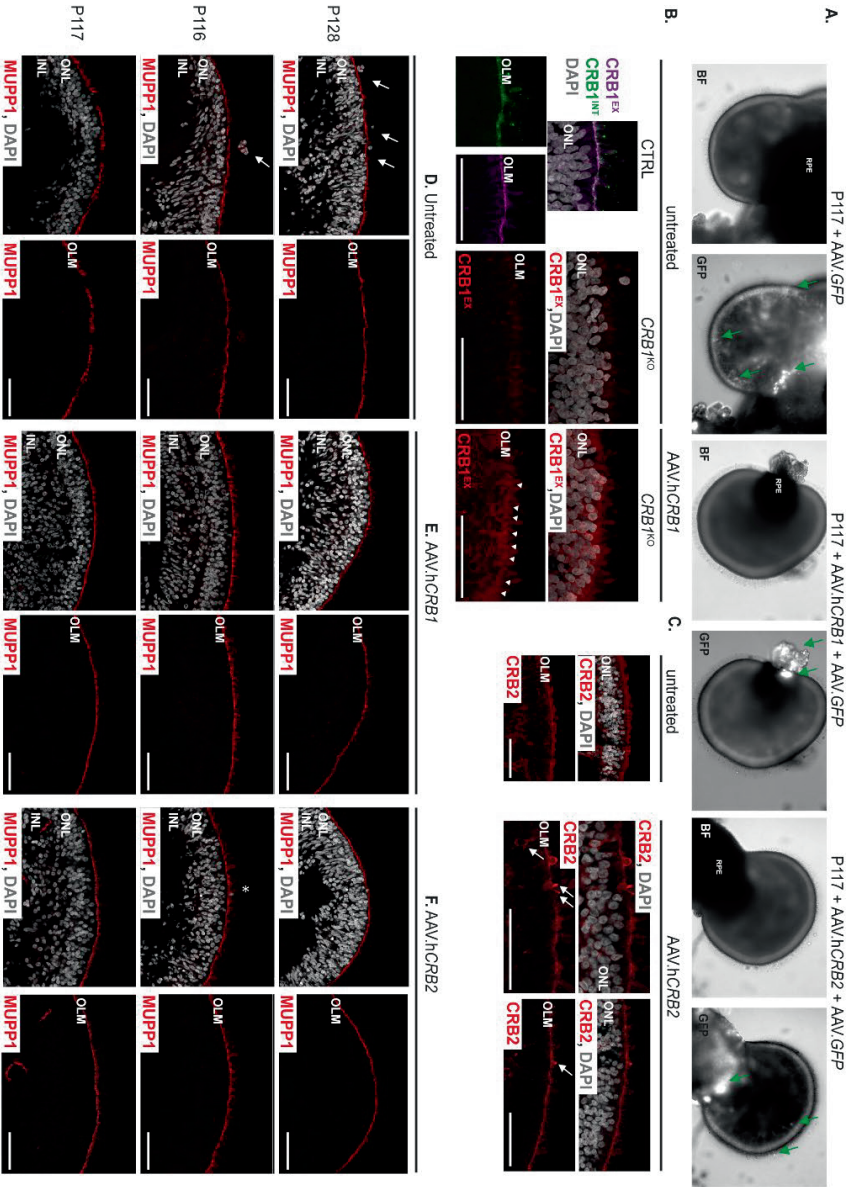
Figure 4 (A–F): AAV-mediated gene therapy treatment on *CRB1* patient-derived and isogenic control retinal organoids.
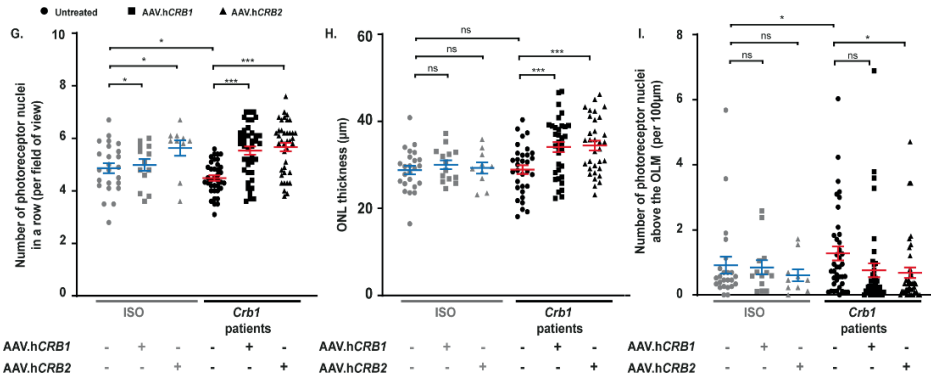
Figure 4 (G-I): AAV-mediated gene therapy treatment on *CRB1* patient-derived and isogenic control retinal organoids. (A) Representative brightfield (BF) and fluorescent (GFP, GFP regions indicated with green arrow) images of DD210 cultured P117 retinal organoids treated with $3,3 \times 10^{10}$ vg AAV.h*CRB*. (B) Immunohistochemical image of CRB1 in untreated control retinal organoid, untreated *CRB1*^{KO} retinal organoid, and AAV.h*CRB1* treated *CRB1*^{KO} retinal organoid showing increased CRB1 localization at the OLM of AAV.h*CRB1* treated *CRB1*^{KO} retinal organoids (arrowheads). (C) Immunohistochemical image of CRB2 in untreated and AAV.h*CRB2* treated *CRB1* patient-derived retinal organoid at the OLM. Arrows indicate overexpression of CRB2 in photoreceptor cells in AAV.h*CRB2* treated retinal organoids. (D, E, F): Representative immunohistochemical images of (D) untreated, (E) AAV.h*CRB1*, and (F) AAV.h*CRB2* treated *CRB1* patient retinal organoids stained with MUPP1 (red) at DD210. (G) Quantification of the number of photoreceptor nuclei in a row (from left to right: $p = 0.000$, $p = 0.000$, $p = 0.039$, $p = 0.046$, $p = 0.046$), (H) ONL thickness ($p = 0.001$, $p = 0.001$, $p = 0,923$, $p = 0.757$, $p = 0.243$) and (I) the number of photoreceptor nuclei above the OLM ($p = 0.116$, $p = 0.034$, $p = 0,0.034$, $p = 0.717$, $p = 0.730$) in three *CRB1* patients and three isogenic control organoids with and without concomitant treatment of AAV.*GFP* pooled. Scalebar = 50μm. Each datapoint in the graph represent individual organoids, of which an average has been taken of at least 3 representative images. The standard error of mean (SEM) is derived from these averages. Number of individual organoids per condition: *CRB1* patients (P116, P117, P128 pooled) treated with AAV.h*CRB1* $n = 34$, AAV.h*CRB2* $n = 33$, untreated and GFP treated $n = 32$, and isogenic controls (ISO-02 P116, ISO-03 P116, ISO-P128 pooled) treated with AAV.h*CRB1* $n = 14$, AAV.h*CRB2* $n = 10$, and untreated and GFP treated $n = 24$ independent organoid from two different differentiation rounds. Statistical tests: generalized linear mixed models with $p < 0.05$ (*), $p < 0.01$ (**), and $p < 0.001$ (***). Related to Supplemental Figure 4.

Altogether, this data show that the phenotype observed at DD180 and DD210 in *CRB1* patient-derived retinal organoids can be partially restored using AAV.h*CRB1* or AAV.h*CRB2* treatment.

Differentially expressed genes related to the endosomal system are partially restored in AAV.hCRB treated CRB1 patient-derived retinal organoids

To identify gene expression changes upon *CRB* gene augmentation therapy, all three *CRB1* patient-derived retinal organoids were treated with AAV.h*CRB1* and AAV.*GFP* or AAV.h*CRB2* and AAV.*GFP* and compared to the AAV.*GFP* treated control at DD230 using scRNA-seq. For all three patient-derived retinal organoids, we confirmed that the major retinal cell clusters were equally present in untreated and AAV treated conditions (data not shown). A custom reference with the AAV.*GFP*, codon optimized AAV.h*CRB1* and codon optimized AAV.h*CRB2* sequence were added to the dataset to detect which cell clusters were transduced. While analyzing all organoids and conditions together, we observed that AAV.*GFP* mainly transduces RPE, photoreceptor cells, transient I, and MGC (Supplemental Figure 5A). Specifically, 66% of the RPE, 35% of Rods, 36% of cones, 37% of transient I and 20% of MGC contained AAV.GFP expression. This is in line with what we previously observed in the immunohistochemical analysis (Figure 3E, F). Next, AAV.h*CRB1* and AAV.h*CRB2* expression was analyzed in AAV.h*CRB* treated retinal organoids. While being unable to fully distinguish exogenous and endogenous h*CRB* due to the high sequence similarity and the low levels of endogenous *CRB1* and *CRB2* in DD230 RPE, we observed a significant increase of AAV.h*CRB1* in AAV.h*CRB1* treated and AAV.h*CRB2* in AAV.h*CRB2* treated organoids in the RPE of the *CRB1* patient-derived retinal organoids (Supplemental Figure 5B, 5C).

Differential gene expression followed by GO term analysis of AAV.h*CRB1* treatment compared to untreated P128 retinal organoids in MGC revealed differences related to the endosomal system, cell-cell adhesion, and protein or receptor binding (Figure 5A). Also for AAV.h*CRB2* treatment similar terms were observed to be statistically significant in P128 (Figure 5C). Next, these GO terms and differentially expressed genes were compared to the ones observed when contrasting P128 with ISO-P128. Overlapping differentially expressed genes associated with the endosomal system show that after AAV.h*CRB1* treatment the expression levels from the patient retinal organoids are similar to levels of the isogenic control (Figure 5B). Moreover, after

AAV.h*CRB2* treatment the genes associated with the endosomal system appeared to be restored as well in MGC (Figure 5D).

Similar comparisons were performed for the other two *CRB1*¬ patient-derived retinal organoids. For P116 and P117, statistically significant GO terms related to the endosomal system were also observed after AAV.h*CRB1* and AAV.h*CRB2* treatment (Supplemental Figure 5D, 5E, 5G, 5I, 5K). When analyzing in more detail the differentially expressed genes associated with the endosomal system in AAV.h*CRB1* treated P116 organoids, transcript levels seemed to be restored to isogenic control levels in MGC (Supplemental Figure 5J) as well as in rod photoreceptor cells (Supplemental Figure 5L). The genes for ISO-P116 indicated with a dashed line box around them were not statistically significant different from P116, but the genes after AAV.h*CRB* treatment are similarly expressed as the average expression in ISO-P116 (Supplemental Figure 5J). Similar results were observed for genes associated with the endosomal system in AAV.h*CRB2* treated organoids (Supplemental Figure 5I). Moreover, after both AAV.h*CRB1* and AAV.h*CRB2* treatment in MGC of P117, we observed that the expression levels changed in a similar direction (Supplemental Figure 5F).

In summary, AAV.h*CRB1* as well as AAV.h*CRB2* treatment on CRB1 patient-derived retinal organoids restores gene expression related to the endosomal system back to isogenic control levels.

Discussion

In this manuscript we have (1) shown diminished levels of variant CRB1 protein in *CRB1* retinitis pigmentosa patient retinal organoids that harbor missense mutations, (2) demonstrated moderate loss of photoreceptors in *CRB1* patient-derived retinal organoids at DD210, (3) detected transcriptional differences suggesting changes within the endosomal system in *CRB1* patient compared to isogenic control organoids, (4) shown that AAV5.CMV.*GFP* efficiently transduced MGCs in addition to photoreceptors and RPE at DD120, and (5) observed a partially restored phenotype after AAV.h*CRB1* or AAV.h*CRB2* mediated gene therapy in *CRB1* patient-derived retinal organoids.
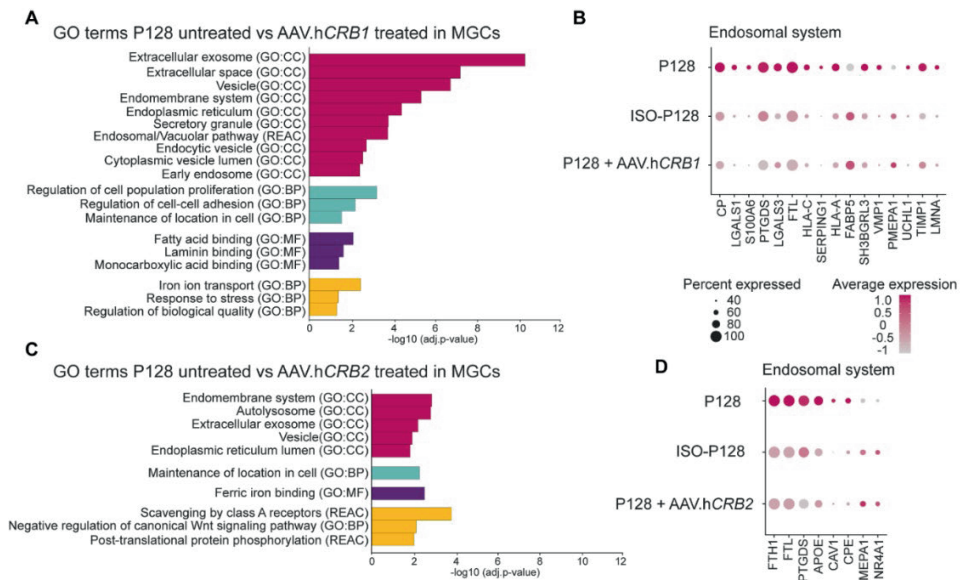
Figure 5: Single cell RNA-sequencing of *CRB1* patient-derived retinal organoid treated with AAV.h*CRB1* or AAV.h*CRB2* restores transcriptional effect on the endosomal system. (A,C) Gene ontology (GO) analysis of differentially expressed markers contrasting untreated with (A) AAV.h*CRB1* or (C) AAV.h*CRB2* treated P128 in MGCs clustered in groups with similar terms in the same colour. (B, D) All significantly differentially expressed markers in terms related to the endosomal system after treatment with (B) AAV.h*CRB1* or (D) AAV.h*CRB2*. All markers present in (B, D) are also statistically significant for P128 compared to ISO-P128. Number of independent organoids used: P128 n = 6, P128 with AAV.h*CRB1* n = 5, P128 with AAV.h*CRB2* n = 5 from one differentiation round equally divided into three separate sequencing rounds. Related to Supplemental Figure 5.

CRB1 patient's clinical and genetic characteristics were described previously in detail in a prospective natural history study on 22 patients [3]. The P116 retinal organoids were derived from skin fibroblasts from a patient with at first diagnosis retinitis pigmentosa and discontinuous outer limiting membrane (OLM) and ellipsoid zone (EZ) in parafovea and perifovea on spectral domain optical coherence tomography (SD-OCT), see supplemental tables 1 and 2 in Nguyen et al 2022. The P117 retinal organoids were derived from a patient that experienced mild retinitis pigmentosa with at first diagnosis loss of visual acuity and continuous OLM and EZ in parafovea and perifovea. The P128 retinal organoids were derived from a patient with at first diagnosis retinitis pigmentosa, nyctalopia, and discontinuous OLM and EZ in parafovea and perifovea.

Here, the *CRB1* patient-derived retinal organoids were compared to corresponding isogenic controls at DD210. We show a decreased number of photoreceptor nuclei in a row and a reduced ONL thickness in the *CRB1* patient-derived retinal organoids compared to the isogenic controls. Decreased levels of variant CRB1 at the OLM of *CRB1* patient-derived retinal organoids might be associated with increased protrusion of photoreceptor cell bodies into the cell culture medium at DD180 [23] and thinning of the photoreceptor outer nuclear layer at DD210 (current manuscript). This process is similar to the complete loss of CRB1 at the OLM in *Crb1* mouse retina which results in protrusion of photoreceptor cell bodies into the subretinal space [8,16] or the loss of CRB2 at the OLM in *Crb2* mouse retina [20].

Moreover, it was shown that CRB1 and CRB2 are present at the OLM of both photoreceptor and MGCs in iPSC-derived retinal organoids [23]. Our scRNA-seq data confirms on the transcriptome, with more *CRB1* expression in MGCs than in photoreceptor cells and more *CRB2* expression in photoreceptor cells than in MGCs. The rather high expression levels of *CRB1* and low levels of *CRB2* in MGCs might be related to the phenotype variation, since mutations in *CRB1* may cause either early onset RP or LCA. Variable low levels of *CRB2* transcripts in MGCs of *CRB1* patients may be involved in the severity of the phenotype. Such a hypothesis would be in strong correlation with our previous studies in mice, that suggests a modifying role for *CRB2* in *CRB1*-related dystrophies [13,14,17,21,26].

CRB1 variant protein at the OLM was strongly diminished in *CRB1* patient-derived retinal organoids, while *CRB1* expression levels remained similar. In contrast, CRB core complex members as well as the FERM proteins remained at the OLM and similar expression levels were observed. This indicates that a variant CRB1 protein is produced but it does not localize to or maintain its expected location at the OLM. The endolysomal system is required for transport of CRB1 to the OLM but also for recycling of endocytosed CRB1 from the early endosome to the OLM and the transport into degradative vesicles. *Drosophila* studies show that Crb trafficking is mediated by transport along microtubules by Rab11- and retromer-containing endosomes [27,28]. In addition, in *Drosophila* salivary gland cells Crumbs maintains the active pool of Rab

proteins at the apical domain, which is essential for maintaining the organization of the apical membrane and efficient apical secretion [29]. The scRNA-seq gene ontology data shown here suggests an aberrant endosomal pathway specifically in MGCs and rods of *CRB1* patient-derived retinal organoids. Dysregulation of CRB1 at the OLM can thus cause changes in the endosomal system. Endosomal recycling is pivotal for maintenance of neuronal health, and defects in its function results in human neurodegenerative disorders [30,31]. We hypothesize that the reduced levels of variant CRB1 at the OLM are caused by disturbed variant CRB1 protein transport to the OLM, or disturbed endosomal recycling of variant CRB1 between OLM and the early endosome, or increased variant CRB1 degradation in the retinal organoids. Preliminary studies suggest changes in the recycling endosome and in degradative vesicles (Buck TM et al Wijnholds J, unpublished results). In analogy to the roles of the Crumbs protein in *Drosophila* salivary glands [29], in future studies we will examine the putative role for CRB1 in the maintenance of an active pool of RAB11 and VPS35 (retromer) recycling endosome proteins at the OLM.

Previously, we described an improved phenotype after AAV.h*CRB2* treatment in *Crb* mutant mouse models [13,14]. Here, we investigated whether we could observe an improved CRB1-RP phenotype after AAV-mediated gene augmentation therapy in *CRB1* patient-derived retinal organoids. Proof-of-concept for developing gene therapy in retinal organoids for CRX-LCA has been described, where AAVs were used to alleviate the phenotype observed in CRX mutant retinal organoids [32]. In addition, AAV-mediated gene augmentation of RP2 knock-out retinal organoids prevents ONL thinning and restored rhodopsin expression [33]. In this manuscript, using AAV.h*CRB1* and AAV.h*CRB2* gene augmentation therapy, a partially restored phenotype was observed in *CRB1* patient-derived retinal organoids. The number of photoreceptor nuclei in a row and ONL thickness were significantly improved after AAV.h*CRB* treatment when analyzed at DD210, showing the long-term effects of the gene augmentation therapy. Moreover, neither positive nor negative effects were observed when treating isogenic controls with AAV.h*CRB1* or AAV.h*CRB2*. Furthermore, the infection of AAV.h*CRB1* on the *CRB1*[KO] retinal organoids show localization of recombinant CRB1 protein at the OLM. Whereas the recombinant CRB1 protein

localizes merely at the OLM, we also detected CRB1 protein around the OLM as previously detected in first trimester human fetal retina and DD120 immature wild type retinal organoids [23]. The imprecise localization of recombinant CRB1 is potentially related to a partial restoration of CRB1-positive recycling endosomal vesicles at the OLM and is subject of future studies. To our knowledge, this is the first time that an improved phenotype after AAV.h*CRB* gene augmentation in *CRB1* patient-derived retinal organoids is observed.

In conclusion, we demonstrate in *CRB1* patient-derived retinal organoids a moderate loss of photoreceptor nuclei in a row, strongly reduced levels of CRB1 variant protein with unaffected *CRB1* transcript levels, and a dysregulated molecular gene profiling phenotype of MGC and rod photoreceptor cells, suggesting an aberrant endosomal system. Moreover, using AAV-mediated gene augmentation therapy approaches we have improved the histological and transcriptional retinal phenotype in *CRB1* patient-derived retinal organoids. These data provide essential information for future gene therapy approaches for patients with mutations in the *CRB1* gene.

Experimental procedures

Cell culture and retinal organoid differentiation

The following hiPSC lines were used for organoid differentiation: three *CRB1* RP patient-derived lines and one control (LUMC0116iCRB09, LUMC0117iCRB01, LUMC0128iCRB01, LUMC0004iCTRL10; [23]), and three isogenic controls of the *CRB1* patient-derived lines (LUMC0116iCRB-ISO02, LUMC0116iCRB-ISO03, LUMC0128iCRB-ISO01) (Supplemental Figure 1, Supplemental Table 1). hiPSC lines were derived from skin fibroblast using polycistronic Lentiviral vectors [34].

hiPSC were maintained on Matrigel coated plates in mTeSR plus medium and passaged mechanically using gentle cell dissociation reagent (STEMCELL Technologies). Retinal organoid differentiation was carried out as previously reported with some modifications (Supplemental experimental procedures) [23,35]. Retinal organoids were collected at DD180 or DD210 for immunohistochemical analysis; a list of all primary

antibodies used for immunofluorescent staining is provided in (Supplemental Table 2). At least three different differentiation batches were analyzed to verify disease phenotypes.

AAV transduction of hiPSC-derived retinal organoids

Two to three retinal organoids were plated in a 96-well agarose coated plate and were infected with AAV in 50 µL RLM2 and incubated for 8h at 5% CO_2 at 37°C. After this, the wells were topped up to 200 µL with RLM2. The next morning, treated organoids were transferred to a 24 well plate and cultured for at least 3 weeks or until the desired differentiation day. AAV5.CMV.*GFP* and AAV2.CMV.*GFP* (105530; Addgene) were used at a titer of $1x10^{10}$, $3.3x10^{10}$, $6.6x10^{10}$, or $10x10^{10}$gc. AAV5.CMVmin.h*CRB1* and AAV5.CMV.h*CRB2* (HORAMA) were used with a titer of $3.3x10^{10}$gc.

Quantification and statistical analysis

40x magnification images were manually quantified using Fiji ImageJ (ImageJ 1.53f51). At least 4 organoids per condition with 3-6 representative images of each organoid were used for quantification. Three regions in each image were manually analyzed for the number of photoreceptor nuclei in a row in the ONL, the number of photoreceptor nuclei above the OLM, retinal thickness, INL thickness, and ONL thickness. Quantifications were performed independently by at least two researchers without the knowledge of genotype or treatment. For the MUPP1 quantifications, a ROI was drawn at the OLM and the average intensity was measured using ImageJ. All datapoints measured were averaged per organoid and plotted in the graph; so that each point is one organoid. No normalization of the values was performed. Data were either presented per 100µm retinal length or per field of view. Data presentation and statistical analysis were performed using GraphPad Prism version 8 (GraphPad Software) and IBM SPSS statistics (version 25), respectively. For statistical analysis, all individual values per image were used. A generalized linear mixed models with treatment (and patient) as a fixed effect was performed on all quantification parameters; the statistical test took into account that multiple *CRB1* patients were merged by introducing a

random intercept per patient. Data is presented as mean per organoid ± standard error of the mean (SEM). Significance is indicated in graphs as $p < 0.05$ (*), $p < 0.01$ (**), and $p < 0.001$ (***).

Single cell RNA sequencing

Retinal organoids were dissociated using an adapted protocol from the Papain Dissociation kit (Worthington, I-LK 03150). Analysis and processing of single-cell transcriptomics using Seurat is detailed in supplemental experimental procedures.

Article information

Author contributions: Conceptualization, N.B. and J.W.; Software, N.B., I.M., S.B. and H.M; Formal analysis, N.B.; Investigation, N.B., X.L., C.A.A, and T.M.B.; Resources, C.J.F.B., C.F., and C.H.A..; Data curation, N.B. and I.M.; Writing – original draft, N.B.; Writing – review & editing, N.B., and J.W.; Visualization, N.B.; Supervision, J.W.; Project administration, J.W.; Funding acquisition, J.W.

Abbreviations

AAV	Adeno-associated viral vectors
CRB1	Crumbs homolog-1
CNV	Copy number variation
CMV	Cytomegalovirus
CRALBP	Cellular retinaldehyde-binding protein
DD210	Differentiation day 210
EGF	Epidermal growth factor
ERLI	Glutamic acid-arginine-leucine-isoleucine
FERM	Protein 4.1, Ezrin, Radixin, Moesin
GFP	Green Fluorescent Protein
GO	Gene ontology
hiPSC	Human-induced pluripotent stem cell
INL	Inner nuclear layer
LCA	Leber congenital amaurosis
MGC	Müller glial cell
MPP5	Membrane-associated guanylate kinase p55 subfamily member 5
MUPP1	Multiple PDZ domain protein 1
NGS	Next Generation Sequencing
OLM	Outer limiting membrane
ONL	Outer nuclear layer
OPL	Outer plexiform layer
OTX2	Orthodenticle Homebox2
PALS1	Protein associated with Lin Seven 1
RHO	Rhodopsin
RP	Retinitis pigmentosa
RPE	Retinal pigment epithelium
RT	Room temperature
RT-qPCR	Reverse transcription quantitative real-time PCR
SAR	Subapical region
scRNA-seq	Single cell RNA-sequencing
SEM	Standard error of mean
SOX9	SRY-Box Transcription Factor 9

References

1.   Den Hollander, A.I.; Ten Brink, J.B.; De Kok, Y.J.M.; Van Soest, S.; Van Den Born, L.I.; Van Driel, M.A.; Van De Pol, D.J.R.; Payne, A.M.; Bhattacharya, S.S.; Kellner, U.; et al. Mutations in a human homologue of Drosophila crumbs cause retinitis pigmentosa (RP12*). Nat. Genet*. **1999**, *23*, 217–221, doi:10.1038/13848.

2.   Talib, M.; van Schooneveld, M.J.; van Genderen, M.M.; Wijnholds, J.; Florijn, R.J.; ten Brink, J.B.; Schalij-Delfos, N.E.; Dagnelie, G.; Cremers, F.P.M.; Wolterbeek, R.; et al. Genotypic and Phenotypic Characteristics of CRB1-Associated

Retinal Dystrophies: A Long-Term Follow-up Study. *Ophthalmology* **2017**, *124*, 884–895, doi:10.1016/j.ophtha.2017.01.047.

3.   Nguyen, X.T.A.; Talib, M.; van Schooneveld, M.J.; Wijnholds, J.; van Genderen, M.M.; Schalij-Delfos, N.E.; Klaver, C.C.W.; Talsma, H.E.; Fiocco, M.; Florijn, R.J.; et al. CRB1-Associated Retinal Dystrophies: A Prospective Natural History Study in Anticipation of Future Clinical Trials. *Am. J. Ophthalmol*. **2022**, *234*, 37–48, doi:10.1016/j.ajo.2021.07.021.

4.   Boon, N.; Wijnholds, J.; Pellissier, L.P. Research Models and Gene Augmentation Therapy for CRB1 Retinal Dystrophies. *Front. Neurosci*. **2020**, *14*, 1–13, doi:10.3389/fnins.2020.00860.

5.   Quinn, P.M.; Pellissier, L.P.; Wijnholds, J. The CRB1 complex: Following the trail of crumbs to a feasible gene therapy strategy. *Front. Neurosci*. **2017**, *11*, doi:10.3389/fnins.2017.00175.

6.   Ray, T.A.; Cochran, K.; Kozlowski, C.; Wang, J.; Alexander, G.; Cady, M.A.; Spencer, W.J.; Ruzycki, P.A.; Clark, B.S.; Laeremans, A.; et al. Comprehensive identification of mRNA isoforms reveals the diversity of neural cell-surface molecules with roles in retinal development and disease. *Nat. Commun*. **2020**, *11*, doi:10.1038/s41467-020-17009-7.

7.   Roh, M.H.; Makarova, O.; Liu, C.J.; Shin, K.; Lee, S.; Laurinec, S.; Goyal, M.; Wiggins, R.; Margolis, B. The Maguk protein, Pals1, functions as an adapter, linking mammalian homologues of crumbs and discs lost. *J. Cell Biol*. **2002**, *157*, 161–172, doi:10.1083/jcb.200109010.

8.   van de Pavert, S.A.; Kantardzhieva, A.; Malysheva, A.; Meuleman, J.; Versteeg, I.; Levelt, C.; Klooster, J.; Geiger, S.; Seeliger, M.W.; Rashbass, P.; et al. Crumbs homologue 1 is required for maintenance of photoreceptor cell polarization and adhesion during light exposure. *J. Cell Sci*. **2004**, *117*, 4169–4177, doi:10.1242/jcs.01301.

9.   Margolis, B. The Crumbs3 polarity protein. *Cold Spring Harb. Perspect. Biol*. **2018**, *10*, 1–9, doi:10.1101/cshperspect.a027961.

10.   Bulgakova, N.A.; Knust, E. The Crumbs complex: From epithelial-cell polarity to retinal degeneration. *J. Cell Sci.* **2009**, *122*, 2587–2596, doi:10.1242/jcs.023648.

11.   Maguire, A.M.; Russell, S.; Wellman, J.A.; Chung, D.C.; Yu, Z.F.; Tillman, A.; Wittes, J.; Pappas, J.; Elci, O.; Marshall, K.A.; et al. Efficacy, Safety, and Durability of Voretigene Neparvovec-rzyl in RPE65 Mutation–Associated Inherited Retinal Dystrophy: Results of Phase 1 and 3 Trials. *Ophthalmology* **2019**, *126*, 1273–1285, doi:10.1016/j.ophtha.2019.06.017.

12.   Pellissier, L.P.; Hoek, R.M.; Vos, R.M.; Aartsen, W.M.; Klimczak, R.R.; Hoyng, S.A.; Flannery, J.G.; Wijnholds, J. Specific tools for targeting and expression

in Müller glial cells. *Mol. Ther. - Methods Clin. Dev.* **2014**, *1*, 14009, doi:10.1038/mtm.2014.9.

13. Pellissier, L.P.; Quinn, P.M.; Henrique Alves, C.; Vos, R.M.; Klooster, J.; Flannery, J.G.; Alexander Heimel, J.; Wijnholds, J. Gene therapy into photoreceptors and Müller glial cells restores retinal structure and function in CRB1 retinitis pigmentosa mouse models. *Hum. Mol. Genet.* **2015**, *24*, 3104–3118, doi:10.1093/hmg/ddv062.

14. Buck, T.M.; Vos, R.M.; Alves, C.H.; Wijnholds, J. AAV-CRB2 protects against vision loss in an inducible CRB1 retinitis pigmentosa mouse mode. *Mol. Ther. Methods Clin. Dev.* **2021**, *20*, 423–441, doi:10.1016/j.omtm.2020.12.012.

15. Pellissier, L.P.; Alves, C.H.; Quinn, P.M.; Vos, R.M.; Tanimoto, N.; Lundvig, D.M.S.; Dudok, J.J.; Hooibrink, B.; Richard, F.; Beck, S.C.; et al. Targeted Ablation of Crb1 and Crb2 in Retinal Progenitor Cells Mimics Leber Congenital Amaurosis. *PLoS Genet.* **2013**, *9*, doi:10.1371/journal.pgen.1003976.

16. van de Pavert, S.A.; Meuleman, J.; Malysheva, A.; Aartsen, W.M.; Versteeg, I.; Tonagel, F.; Kamphuis, W.; McCabe, C.J.; Seeliger, M.W.; Wijnholds, J. A single amino acid substitution (Cys249Trp) in Crb1 causes retinal degeneration and deregulates expression of pituitary tumor transforming gene Pttg1. *J. Neurosci.* **2007**, *27*, 564–573, doi:10.1523/JNEUROSCI.3496-06.2007.

17. Quinn, P.M.; Mulder, A.A.; Henrique Alves, C.; Desrosiers, M.; de Vries, S.I.; Klooster, J.; Dalkara, D.; Koster, A.J.; Jost, C.R.; Wijnholds, J. Loss of CRB2 in Müller glial cells modifies a CRB1-associated retinitis pigmentosa phenotype into a Leber congenital amaurosis phenotype. *Hum. Mol. Genet.* **2019**, *28*, 105–123, doi:10.1093/hmg/ddy337.

18. Alves, C.H.; Boon, N.; Mulder, A.A.; Koster, A.J.; Jost, C.R.; Wijnholds, J. CRB2 Loss in Rod Photoreceptors Is Associated with Progressive Loss of Retinal Contrast Sensitivity. *Int. J. Mol. Sci.* **2019**, *20*, 4069, doi:10.3390/ijms20174069.

19. Mehalow, A.K.; Kameya, S.; Smith, R.S.; Hawes, N.L.; Denegre, J.M.; Young, J.A.; Bechtold, L.; Haider, N.B.; Tepass, U.; Heckenlively, J.R.; et al. CRB1 is essential for external limiting membrane integrity and photoreceptor morphogenesis in the mammalian retina. *Hum. Mol. Genet.* **2003**, *12*, 2179–2189, doi:10.1093/hmg/ddg232.

20. Alves, C.H.; Bossers, K.; Vos, R.M.; Essing, A.H.W.; Swagemakers, S.; Van Der Spek, P.J.; Verhaagen, J.; Wijnholds, J. Microarray and morphological analysis of early postnatal CRB2 mutant retinas on a pure C57BL/6J genetic background. *PLoS One* **2013**, *8*, 1–17, doi:10.1371/journal.pone.0082532.

21. Quinn, P.M.; Alves, C.H.; Klooster, J.; Wijnholds, J. CRB2 in immature photoreceptors determines the superior-inferior symmetry of the developing retina to

4

maintain retinal structure and function. *Hum. Mol. Genet*. **2018**, *27*, 3137–3153, doi:10.1093/hmg/ddy194.

22.   van Rossum, A.G.S.H.; Aartsen, W.M.; Meuleman, J.; Klooster, J.; Malysheva, A.; Versteeg, I.; Arsanto, J.P.; Le Bivic, A.; Wijnholds, J. Pals1/Mpp5 is required for correct localization of Crb1 at the subapical region in polarized Müller glia cells. *Hum. Mol. Genet*. **2006**, *15*, 2659–2672, doi:10.1093/hmg/ddl194.

23.   Quinn, P.M.; Buck, T.M.; Mulder, A.A.; Ohonin, C.; Alves, C.H.; Vos, R.M.; Bialecka, M.; van Herwaarden, T.; van Dijk, E.H.C.; Talib, M.; et al. Human iPSC-Derived Retinas Recapitulate the Fetal CRB1 CRB2 Complex Formation and Demonstrate that Photoreceptors and Müller Glia Are Targets of AAV5. *Stem Cell Reports* **2019**, *12*, 906–919, doi:10.1016/j.stemcr.2019.03.002.

24.   Assou, S.; Girault, N.; Plinet, M.; Bouckenheimer, J.; Sansac, C.; Combe, M.; Mianné, J.; Bourguignon, C.; Fieldes, M.; Ahmed, E.; et al. Recurrent Genetic Abnormalities in Human Pluripotent Stem Cells: Definition and Routine Detection in Culture Supernatant by Targeted Droplet Digital PCR. *Stem Cell Reports* **2020**, *14*, 1–8, doi:10.1016/j.stemcr.2019.12.004.

25.   Swaroop, A.; Kim, D.; Forrest, D. Transcriptional regulation of photoreceptor development and homeostasis in the mammalian retina. *Nat. Rev. Neurosci*. **2010**, *11*, 563–576, doi:10.1038/nrn2880.

26.   Pellissier, L.P.; Lundvig, D.M.S.; Tanimoto, N.; Klooster, J.; Vos, R.M.; Richard, F.; Sothilingam, V.; Garrido, M.G.; Bivic, A. Le; Seeliger, M.W.; et al. CRB2 acts as a modifying factor of CRB1-related retinal dystrophies in mice. *Hum. Mol. Genet*. **2014**, *23*, 3759–3771, doi:10.1093/hmg/ddu089.

27.   Aguilar-Aragon, M.; Fletcher, G.; Thompson, B.J. The cytoskeletal motor proteins Dynein and MyoV direct apical transport of Crumbs. *Dev. Biol*. **2020**, *459*, 126–137,   doi:10.1016/j.ydbio.2019.12.009.

28.   Pocha, S.M.; Wassmer, T.; Niehage, C.; Hoflack, B.; Knust, E. Retromer controls epithelial cell polarity by trafficking the apical determinant crumbs. *Curr. Biol*. **2011**, *21*, 1111–1117, doi:10.1016/j.cub.2011.05.007.

29.   Lattner, J.; Leng, W.; Knust, E.; Brankatschk, M.; Flores-Benitez, D. Crumbs organizes the transport machinery by regulating apical levels of pi (4,5)p2 in drosophila. *Elife* **2019**, *8*, 1–45, doi:10.7554/eLife.50900.

30.   Saitoh, S. Endosomal Recycling Defects and Neurodevelopmental Disorders. *Cells* **2022**, *11*, doi:10.3390/cells11010148.

31.   Tang, F.L.; Erion, J.R.; Tian, Y.; Liu, W.; Yin, D.M.; Ye, J.; Tang, B.; Mei, L.; Xiong, W.C. VPS35 in dopamine neurons is required for endosome-to- golgi retrieval of Lamp2a, a receptor of chaperone- mediated autophagy that is critical for α-synuclein degradation and prevention of pathogenesis of Parkinson's disease. *J. Neurosci*. **2015**, *35*, 10613–10628, doi:10.1523/JNEUROSCI.0042-15.2015.

32.   Kruczek, K.; Qu, Z.; Gentry, J.; Fadl, B.R.; Gieser, L.; Hiriyanna, S.; Batz, Z.; Samant, M.; Samanta, A.; Chu, C.J.; et al. Gene Therapy of Dominant CRX-Leber Congenital Amaurosis using Patient Stem Cell-Derived Retinal Organoids. *Stem Cell Reports* **2021**, *16*, 252–263, doi:10.1016/j.stemcr.2020.12.018.

33.   Lane, A.; Jovanovic, K.; Shortall, C.; Ottaviani, D.; Panes, A.B.; Schwarz, N.; Guarascio, R.; Hayes, M.J.; Palfi, A.; Chadderton, N.; et al. Modeling and Rescue of RP2 Retinitis Pigmentosa Using iPSC-Derived Retinal Organoids. *Stem Cell Reports* **2020**, *15*, 67–79, doi:10.1016/j.stemcr.2020.05.007.

34.   Warlich, E.; Kuehle, J.; Cantz, T.; Brugman, M.H.; Maetzig, T.; Galla, M.; Filipczyk, A.A.; Halle, S.; Klump, H.; Schöler, H.R.; et al. Lentiviral vector design and imaging approaches to visualize the early stages of cellular reprogramming. *Mol. Ther*. **2011**, *19*, 782–789, doi:10.1038/mt.2010.314.

35.   Zhong, X.; Gutierrez, C.; Xue, T.; Hampton, C.; Vergara, M.N.; Cao, L.H.; Peters, A.; Park, T.S.; Zambidis, E.T.; Meyer, J.S.; et al. Generation of three-dimensional retinal tissue with functional photoreceptors from human iPSCs. *Nat. Commun.* **2014**, *5*, doi:10.1038/ncomms5047.

4

Supplemental information
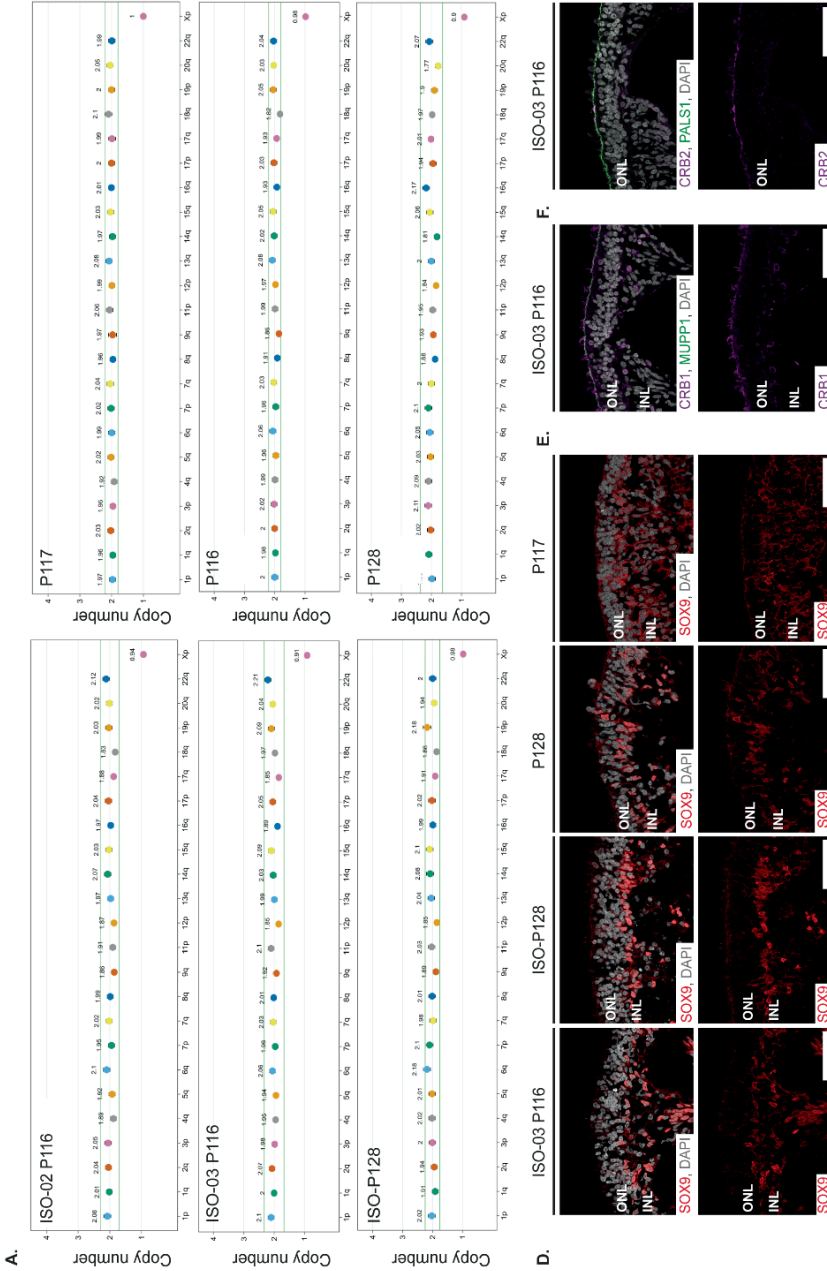
Supplemental Figure 1 (A, D-F): *CRB1* **patient derived and isogenic control retinal organoids phenotypic analysis at DD210.** Related to Figure 1. (A) Meta-analysis of 90% most recurrent abnormalities in hiPSCs showing no abnormalities after creating the isogenic controls used in this study. *Legend continues on the next page*
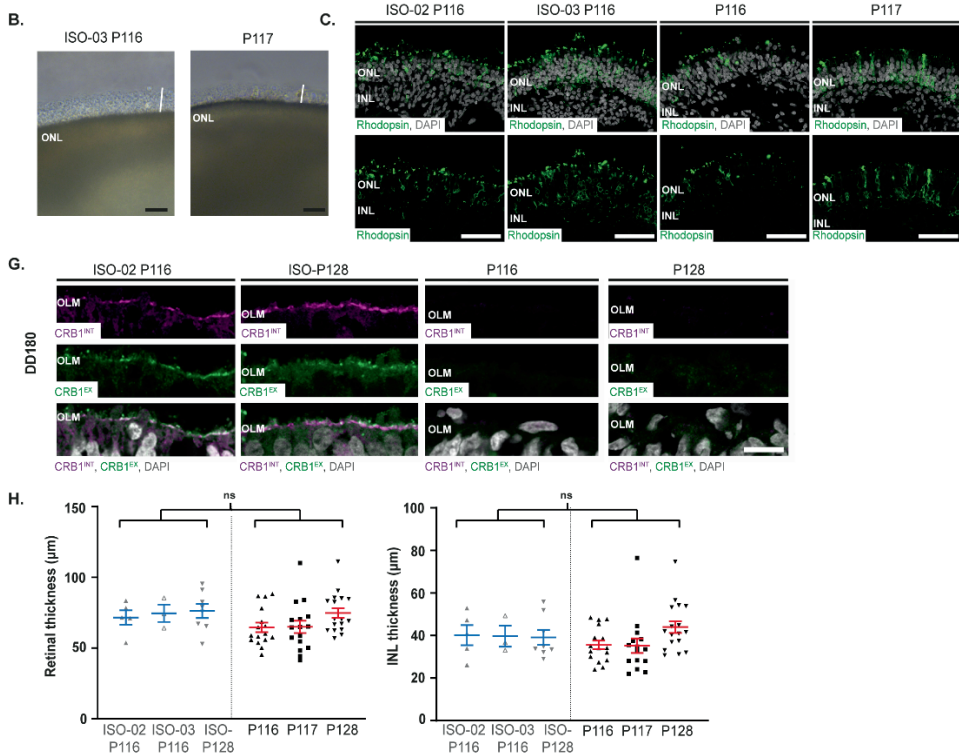
Supplemental Figure 1 (B, C, G, H): *CRB1* **patient derived and isogenic control retinal organoids phenotypic analysis at DD210.** (B) Representative brightfield images of ISO-03 P116 and P117 cultured organoids. (C) Representative immunohistochemical images of rhodopsin (green) in ISO-02 P116, ISO-03 P116, P116, and P117. (D) Representative immunohistochemical images of SOX9 (red) in ISO-P128, P128, P117, and ISO-03 P116. (E, F) Representative immunohistochemical images of (E) CRB1 (magenta) co-localized with MUPP1 (green) and of (F) CRB2 (magenta) co-localized with PALS1 (green) in ISO-03 P116. (G) Representative immunohistochemical images of CRB1^{EX} (green) and CRB1^{INT} (magenta) in *CRB1* patient-derived retinal organoids compared to isogenic controls at DD180. (H) Quantitative analysis of the total retinal thickness ($p = 0.158$) and INL thickness ($p = 0.696$) per field of view in *CRB1* patient derived and isogenic control retinal organoids. Each datapoint in the graph represent individual organoids, of which an average has been taken of at least 3 representative images. The standard error of mean (SEM) is derived from these averages. Number of individual organoids per condition and differentiation round: P116 $n = 16$, P117 $n = 15$, P128 $n = 17$ from four independent organoid batches, ISO-P128 $n = 8$ from three independent organoid batches, ISO-02 P116 $n = 5$ and ISO-03 P116 $n = 5$ from two independent organoid batches. Scalebar = (C-F) 50µm, (G) 10µm.

4
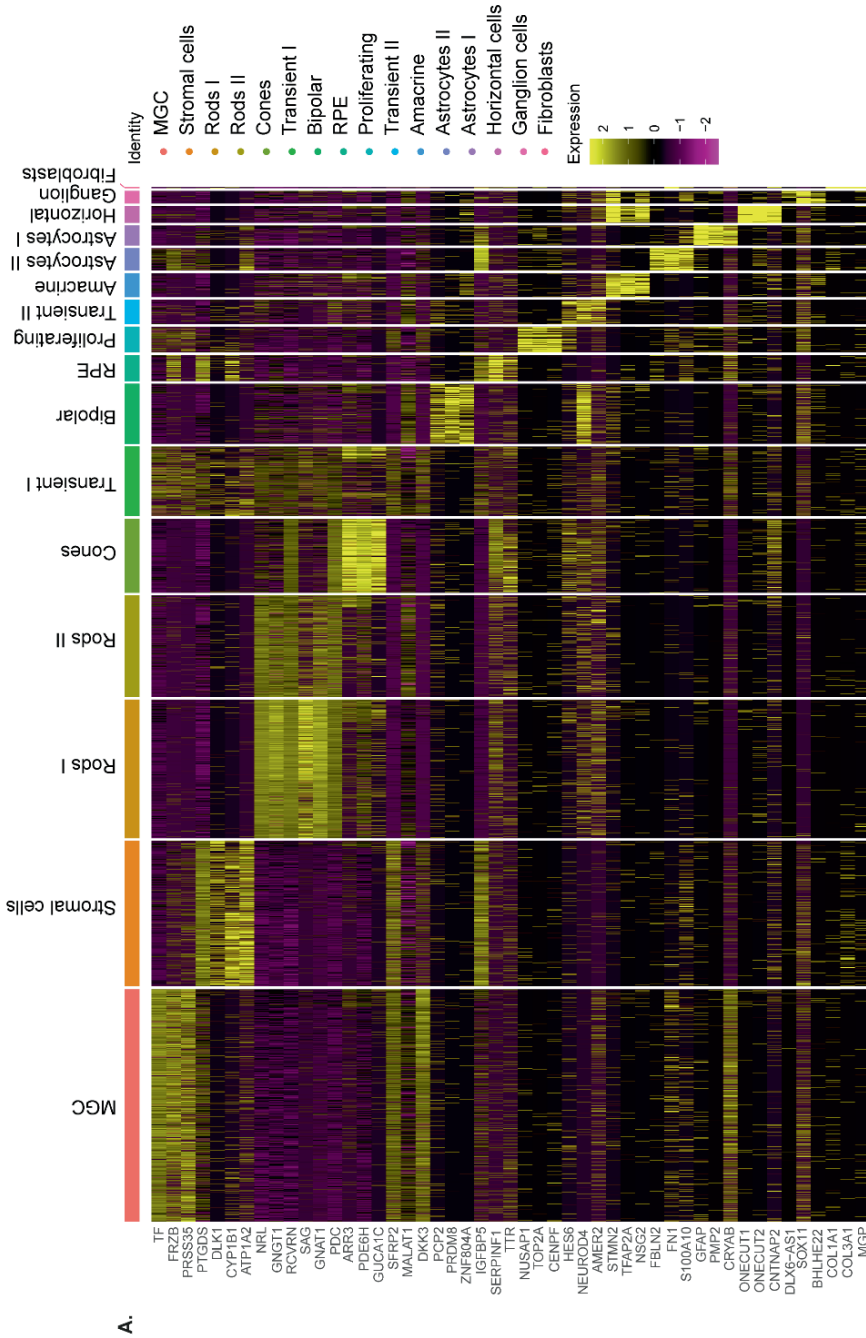
Supplemental Figure 2 (A): scRNA-seq analysis comparing ISO-P128 with P128. (A) Heatmap of top markers indicating the distinct clusters.
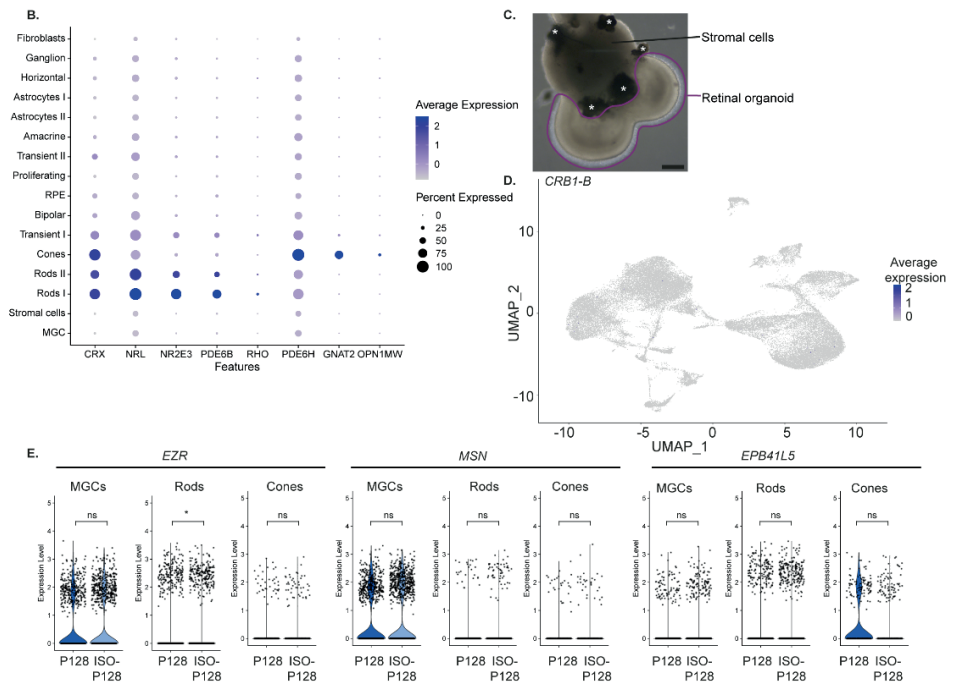
Supplemental Figure 2: scRNA-seq analysis comparing ISO-P128 with P128. Related to Figure 2. (B) Dot-plot showing higher expression of mature rod photoreceptor cell features in rods I then in rods II cluster. (C) Overview of a retinal organoid in culture with RPE (asterisks) and stromal cells attached to it. When using the organoid for single cell sequencing, the stromal cells and RPE were cut off as much as possible. Scalebar 200 µm. (D) Feature plot showing the absence of CRB1 alternative transcript *CRB1-B* in these retinal organoids. (E) Violin plots of *Ezrin* (*EZR*), *Moesin* (*MSN*), and *EPB41L5* specifically in MGCs (from left to right: $p = 0.41$, $p = 0.17$, $p = 0.59$), rods ($p = 0.018$, $p = 0.89$, $p = 0.53$) and cones ($p = 0.77$, $p = 0.79$, $p = 0.24$) in P128 vs ISO-P128. Number of independent organoids used: ISO-P128 $n = 6$, and P128 $n = 6$ from one differentiation round equally divided into three separate sequencing rounds.
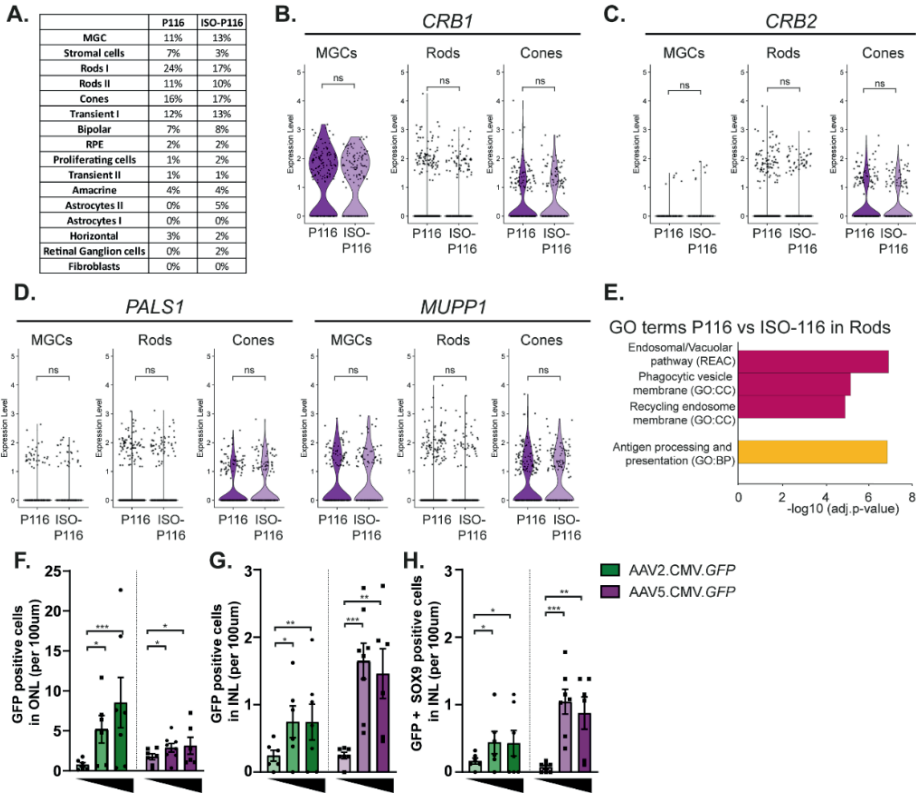
Supplemental Figure 3: scRNA-seq analysis comparing ISO-P116 and P116 retinal organoids. Related to Figure 2. (A) Table showing all retinal cell types equally present in the retinal organoids. (B) Violin plots of *CRB1* and (C) *CRB2* expression levels specifically in MGCs ($p = 0.78$, $p = 0.28$), rods ($p = 0.37$, $p = 0.88$), and cones ($p = 0.51$, $p = 0.96$). (D) Violin plots of canonical core CRB complex members *PALS1*, and *MUPP1* transcripts in MGCs ($p = 0.49$, $p = 0.98$), rods ($p = 0.36$, $p = 0.61$), and cones ($p = 0.41$, $p = 0.86$). (E) Gene ontology (GO) analysis of differentially expressed markers specifically in rods clustered with similar terms in the same colour. Number of independent organoids used: ISO-P116 $n = 4$, and P116 $n = 4$ from one differentiation and sequencing round. (F, G, H) Quantification of AAV2.CMV.*GFP* and AAV5.CMV.*GFP* retinal organoids at DD120 with three different titre concentrations: $1x10^{10}$, $6.6x10^{10}$, and $10x10^{10}$ gc (genome copies) in the (F) ONL, (G) INL, and (H)) GFP positive MGC in the INL per 100µm. Each datapoint in the graph represent individual organoids, of which an average has been taken of at least 3 representative images. The standard error of mean (SEM) is derived from these averages. Number of organoids per condition: for AAV2.CMV.*GFP* $1x10^{10}$ $n = 5$, $6.6x10^{10}$ $n = 6$, and $10x10^{10}$ $n = 7$, and for AAV5.CMV.*GFP* $1x10^{10}$ $n = 7$, $6.6x10^{10}$ $n = 8$, and $10x10^{10}$ $n = 6$ individual organoids from two independent differentiation rounds. Statical analysis: generalized linear mixed models with $p < 0.05$ (*), $p < 0.01$ (**), and $p < 0.001$ (***).
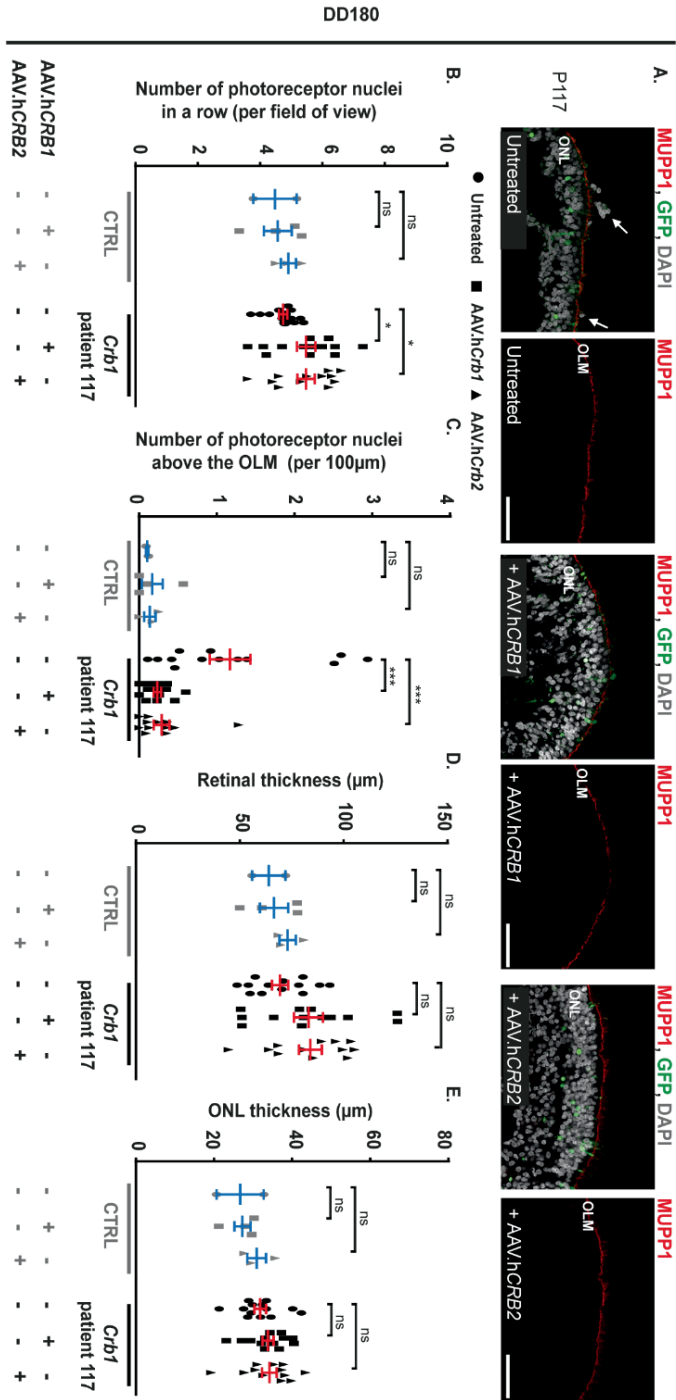
Supplemental Figure 4: AAV-mediated gene therapy treatment on *CRB1* patient-derived and isogenic control retinal organoids (A–E). Related to Figure 4. (A) Representative immunohistochemical images of untreated, AAV.hCRB1, and AAV.hCRB2 treated P117 and control retinal organoids stained with MUPP1 (red) and AAV.GFP (green) at DD180. (B) Quantification at DD180 of the number of photoreceptor nuclei in a row per field of view (from left to right: $p = 0.042, p = 0.041, p = 0.925, p = 0.548$), (C) the number of photoreceptor nuclei above the OLM per 100 μm ($p = 0.000, p = 0.001, p = 0.676, p = 0.865$), (D) retinal thickness per field of view ($p = 0.104, p = 0.078, p = 0.819, p = 0.389$), and (E) ONL thickness per field of view ($p = 0.438, p = 0.355, p = 0.933, p = 0.378$).

4

Supplemental Figure 4 (F-N): AAV-mediated gene therapy treatment on *CRB1* patient-derived and isogenic control retinal organoids.

Legend continues on the next page

Supplemental Figure 4: AAV-mediated gene therapy treatment on *CRB1* patient-derived and isogenic control retinal organoids. Related to Figure 4. (F) Representative immunohistochemical images of anti-*CRB1*^{EX} and anti-*CRB1*^{INT} showing localization in the RPE after AAV.h*CRB1* treatment in *CRB1* patient-derived retinal organoid. (G) Immunohistochemical image of anti-CRB1^{INT} showing localization at the OLM after AAV.h*CRB1* treatment in *CRB1*^{KO} retinal organoid. (H, I) Representative immunohistochemical images of CRB2 at the (H) OLM and (I) RPE after AAV.h*CRB2* treatment in *CRB1* patient-derived retinal organoids. (J) Quantification of the average MUPP1 fluorescence intensity at the OLM of DD210 *CRB1* patient derived retinal organoids (P116, P117, P128 pooled) treated with AAV.h*CRB*. (K) Representative immunohistochemical images of PALS1 at the OLM with and without AAV.h*CRB* treatment in a *CRB1* patient-derived retinal organoid. (L) Quantification of the retinal thickness ($p = 0.008$, $p = 0.082$, $p = 0.993$, $p = 0.981$, $p = 0.981$) and (M) the INL thickness ($p = 0.139$, $p = 0.632$, $p=0.958$, $p = 0.195$, $p = 0.707$) per field of view of *CRB1* patient and isogenic control retinal organoids at DD210. (N) SDS-PAGE gel of AAV.h*CRB1* and AAV.h*CRB2* showing no contamination in the AAV preparation. Scalebar = 50µm. Each datapoint in the graph represent individual organoids, of which an average has been taken of at least 3 representative images. The standard error of mean (SEM) is derived from these averages. Number of individual organoids per condition at DD180 P117 treated with AAV.h*CRB1* $n = 13$, AAV.h*CRB2* $n = 12$, untreated $n = 14$ from two different differentiation rounds, control organoids treated with AAV.h*CRB1* $n = 4$, AAV.h*CRB2* $n = 3$, and untreated $n = 2$ from one differentiation round. And at DD210 *CRB1* patient-derived retinal organoids (P116, P117, P128 pooled) treated with AAV.h*CRB1* $n = 34$, AAV.h*CRB2* $n = 33$, untreated $n = 32$, and isogenic controls (ISO-02 P116, ISO-03 P116, ISO-P128 pooled) treated with AAV.h*CRB1* $n = 14$, AAV.h*CRB2* $n = 10$, and untreated $n=24$ independent organoid from two different differentiation rounds. Statistical tests: generalized linear mixed models with $p < 0.05$ (*), $p < 0.01$ (**), and $p < 0.001$ (***).

4

Supplemental Figure 5: Single cell RNA-sequencing of *CRB1* patient-derived retinal organoid treated with AAV.h*CRB1* or AAV.h*CRB2* restores transcriptional effect on the endosomal system. Related to Figure 5. (A) Heatmap showing AAV.*GFP* expression in the clusters, mainly transducing MGC, photoreceptor cells, and RPE. (B, C) Violin plot of transcript

expression of (B) AAV.h*CRB1* (from left to right: $p = 0.018$, $p = 0.41$, $p = 0.041$, $p = 0.078$, $p < 0.001$, $p = 0.54$) or (C) AAV.h*CRB2* ($p = 0.5$, $p = 0.1$, $p = 0.38$, $p = 0.0037$, $p = 0.53$, $p < 0.00001$) in the RPE of AAV.h*CRB* treated retinal organoids. (D, E) Gene ontology (GO) analysis of differentially expressed markers contrasting untreated with (D) AAV.h*CRB1* or (E) AAV.h*CRB2* treated P117 in MGCs clustered in groups with similar terms in the same colour. (F) All significantly differentially expressed markers in terms related to the endosomal system after treatment with AAV.h*CRB1* orAAV.h*CRB2* in MGC. (G, H) P117 treated with AAV.h*CRB1* in rods showing gene ontology (G) and all terms related to the endosomal system (H). (I) GO of P116 treatment with AAV.h*CRB* in MGC and (J) dot plot of terms related to the endosomal system after treatment. The data in the box with a dashed line are not statistically significant different from P116, all the other data points (in F, H, J, and L) are statistically significant different from untreated patient derived retinal organoids. Number of independent organoids used: P116 $n = 4$, P116 with AAV.h*CRB1* $n = 3$, P116 with AAV.h*CRB2* $n = 3$ from one differentiation and sequencing round, and P117 $n = 5$, P117 with AAV.h*CRB1* $n = 5$, P117 with AAV.h*CRB2* $n = 5$ from one differentiation round equally divided into three separate sequencing rounds.

Supplemental Table 1. hiPSC line information. Related to all figures.

Line name [published]	Description	Gender
LUMC04iCTRL10 [1]	Control iPSC line	Male
CRB1^{KO}LUMC04iCTRL10	*CRB1*^{KO} line was derived from LUMC04iCTRL10; it has a stop codon in the second exon of *CRB1*. Only used here for proof of recombinant CRB1 protein expression after AAV.h*CRB1* treatment.	Male
LUMC0116iCRB09 [1]	<u>P116</u> = Allele 1 and 2: homozygous c.3122T>C--> p.(Met1041Thr)	Male
iso02LUMC0116iCRB09	<u>ISO-02 P116</u> = Allele 1: c.3122T>C gene corrected to c.3120C>G. Allele 2: c.3122T>C. p.(Met1041Thr)	Male
iso03LUMC0116iCRB09	<u>ISO-03 P116</u> = Homozygous c.3122T>C gene corrected to c.3120C>G	Male
LUMC0117iCRB01 [1]	<u>P117</u> = Allele 1: c.1892A>G (p.Tyr631Cys)). Allele 2: c.2911G>T (p.(Glu995*)	Male
LUMC0128iCRB01 [1]	<u>P128</u> = Allele 1: c.2843G>A --> p.(Cys948Tyr). Allele 2: c.3122T>C --> p.(Met1041Thr)	Male
iso02LUMC0128iCRB01	<u>ISO-P128</u> = Allele 1: c.2843G>A. p.(Cys948Tyr). Allele 2: c.3122T>C gene corrected to c.3120C>G	Male

4

Supplemental Table 2. List of primary antibodies used in the study. Related to all figures.

Antigen	Dilution	Source	Identifier
CRB1 (intracellular domain – used if not otherwise specified)	1:200	Homemade	NA
CRB1 (extracellular domain)	1:200	Abnova	H00023418-A01
CRB2	1:200	Homemade	NA
CRALBP	1:200	Abcam	Ab15051
MUPP1	1:200	BD Biosciences	M98820
PALS1	1:200	Homemade	NA
OTX2	1:200	Proteintech	13497-1-AP
Rhodopsin	1;200	Sigma	SAB4502636
Glutamine synthetase (GS)	1:250	BD Bioscience	610518
SOX9	1:250	Millipore	AB5535

Supplemental Table 3. Top 10 DEG differentially expressed genes per cluster. Related to Figure 2. Statistically significant log2 fold changes of the expression level of differentially expressed genes in the cluster (pct1) comparing with the remaining clusters (pct2). With the defined cell type per cluster. This table is not included in this thesis, due to the large size, and can be found online [6].

Supplemental Table 4. Differentially expressed genes EG markers and gene ontology terms contrasting P128 and ISO-P128, and P116 and ISO-P116. Related to Figure 2, S3A-E. Log2 fold changes of the expression level of statistically significant expressed genes in CRB1 patient-derived retinal organoids comparing with the isogenic control in MGCs or in rod photoreceptor cells and the associated gene ontology terms. This table is not included in this thesis, due to the large size, and can be found online [6].

Supplemental Table 5. DEG markers and gene ontology terms comparing untreated and AAV.hCRB treated CRB1 patient derived retinal organoids. Related to Figure 5, S5. Log2 fold changes of the expression level of statistically significant expressed genes in AAV.hCRB treated CRB1 patient-derived retinal organoids comparing with the untreated and the associated gene ontology terms. This table is not included in this thesis, due to the large size, and can be found online [6].

Supplemental experimental procedures

Cell culture and retinal organoid differentiation

Human induced pluripotent stem cells (hiPSC) were maintained on Matrigel coated plates in mTeSR plus medium (STEMCELL Technologies) and passaged mechanically. Retinal organoid differentiation was carried out as previously reported

with some modifications [1,2]. Confluent hiPSCs were collected and incubated with (±)blebbistatin in mTeSR medium in micro-mold spheroids (Z764000-6EA, Merck) over night. Then, medium was transitioned to Neural Induction Medium 1 (NIM1) using mTeSR/NIM1 (3:1), then (1:1), and finally (0:1) over three days to form embryoid bodies (EBs). After 1 week, EBs were plated onto Matrigel-coated wells with daily NIM-1 medium change till DD15 and daily change of NIM-2 starting at DD16. Between DD20 and latest DD28, neuroepithelial structures were selected and flushed from the Matrigel plates using a P1000 pipet and kept in floating culture in agarose coated plates from this point onwards. After selecting the best-looking structures, all structures were flushed from the Matrigel plates and kept in floating culture to increase the yield of obtained organoids. Then, typically from DD40 until DD100, good retinal organoid structures were selected and placed individually in a 48 well plate. Brain and other non-retinal structures were removed as well between this time period. Daily medium change of NIM-2 is used till DD34, then typically three times a week Retinal Lamination Medium 1 (RLM-1) was used from DD35 to DD63. Then, RLM-1 + 1µM retinoic acid until DD84, followed by RLM-2 + 0.5µM retinoic acid, and RLM-2 from DD120 was used for the rest of the culture.

Immunohistochemical analysis

Organoids were collected at DD180 or DD210 for immunohistochemical analysis. Organoids were fixed with 4% paraformaldehyde in PBS for 20 minutes at RT, briefly washed with PBS and subsequently cryo-protected with 15% and 30% sucrose in PBS until organoids sunk to the bottom of the well. Organoids were embedded in Tissue-Tek O.C.T. Compound (Sakura, Finetek), thereafter 8 µM cryosections were made with a Leica CM1900 cryostat (Leica Microsystems) and stored in the freezer.

For immunohistochemistry, the sections were blocked for 1h at RT in 10% normal goat serum, 0.4% Triton X-100, and 1% bovine serum albumin in PBS. Primary antibodies were incubated overnight at 4°C or for at least 3h at RT with 0.3% normal goat serum, 0.4% Triton X-100, 1% BSA and appropriate primary antibody concentration (Supplemental Table 2). Then, slides were washed for two times 15 minutes in PBS and subsequently incubated for 1h at RT with fluorescent-labelled secondary antibody

in 0.1% goat serum in PBS. Nuclei were counterstained with DAPI and mounted in Vectashield Hardset mounting medium (H1800, Vector laboratories, Burlingame, USA). Sections were imaged on a Leica TCS SP8 confocal microscope and images were processed with Leica Application suite X (v3.7.0.20979).

RNA isolation, cDNA synthesis, and qPCR analysis

RNA was isolated from DD210 retinal organoids of P116, P117, P128, ISO-P128, and ISO-02 P116 using TRIZOL reagent (Gibco Life Technologies) according to the manufacturer manual. The isolated RNA was dissolved in 20µl RNase-free water. 0.5µg of total RNA was reverse transcribed into first-strand cDNA using QuantiTect Reverse Transcription Kit (205311, QIAGEN) in a total reaction volume of 20µl. From all cDNA samples, a 1 in 20 dilution was made and used for qPCR analysis.

Two different exon-spanning primer pairs were designed at the 5' end of the CRB1-B gene giving rise to an amplicon of 70 to 120bp (FW1: TGTTTGGAGCCAGGACACAT, REV1: ACGTCTTCTTCGCAGTGGAT and FW2: GAGCCAGGACACATGGTTTTC, REV2: TTCCCAGGCAAGTTCTCACA). Real-time qPCR was based on the monitoring of SYBR Green I dye fluorescence on a CFX Connect Real-Time System (BioRad). The qPCR conditions were as follows: 5µl SYBR green PCR 2x master mix (4913914001, Merck), 0.2µl of 10µM FW and REV primers, and 5ul of the diluted cDNA. qPCR machine started with a melting step at 95°C for 10min, followed by 40 cycles of 95°C for 15 seconds and an annealing at 60°C for one minute. At the end of the PCR run, a dissociation curve was determined by ramping the temperature of the sample from 60 to 95°C while continuously collecting fluorescence data. MQ water controls were included for each primer pair to check for any significant levels of contaminants. The following two reference genes were used: glyceraldehyde 3-phosphate dehydrogenase (GAPDH) and elongation factor 1a (EF1A), previously described by [3].

qPCR was performed on both primer pairs with at least three individual DD210 retinal organoids of P116, P117, P128, ISO-P128, and ISO-02 P116 cDNA and human adult retina cDNA (Marathon-ready; Clontech). CRB1-B was detected in adult human retina

cDNA but was below detection level in the patient-derived and isogenic control retinal organoids at DD210.

Single cell RNA sequencing – Retinal organoid dissociation

Retinal organoids were dissociated using an adapted protocol from the Papain Dissociation kit (Worthington, I-LK 03150). In short, single retinal organoids were selected and cut into small pieces to remove excess RPE or non-neural tissue as much as possible and placed on a 48 well plate with 500µl dissociation solution (20 units/ml papain and 0.005% DNase). These were incubated for 30 minutes on a shaker in the incubator, then the organoids were triturated using a 1mL pipettor to dissociate the tissue. The plate was placed back for 15-20 minutes on the shaker in the incubator, then again triturated, this was repeated until a single cell suspension was obtained. 500µl albumin ovomucoid protease inhibitor solution was added to the single cell suspension, centrifuged at 300x g for 5min. Supernatant was removed, pellet resuspend in PBS and filtered through a 40um cell strainer (Pluristrainer; SKU 43-10040-50).

Filtered single cell suspension was centrifuged at 300x g for 5min at 4˚C and resuspend in 100µl staining buffer (2%BSA/0.01%Tween, PBS) with 10µl Fc Blocking reagent (FcX, BioLegend) for 10 minutes on ice. 0.5µg of unique Cell Hashing antibodies were added and incubated for 20 minutes on ice. Stained cells were washed 3 times with 1mL staining buffer, spinned at 4 ˚C for 5 minutes at 350g. Stained single cell suspensions were counted for cell concentration and cell viability (TC20, Bio-rad). Typically, all single cell suspensions had a 70% or higher cell viability. Stained cells were pooled and re-counted until desired concentration for single cell sequencing (cell viability of at least 80%). Every sequencing round contained 14 hashed retinal organoid samples; the goal was to capture a total of approximately 30.000 cells per pool.

Single cell RNA sequencing – Droplet-based single-cell RNA sequencing

ScRNA-seq data was generated using the Chromium 10x 3'UTR-sequencing. Single cell suspensions were loaded onto the Chromium Single Cell system using the v3 chemistry. Subsequent steps were performed according to manufacturer's instructions.

Single cell RNA sequencing – Computational analysis of single cell data

Raw sequencing output were processed using the Cell Ranger (v6.0.1) pipeline (10X Genomics) with default settings and the pre-built human genome reference (GRCh38). Custom references of codon optimized AAV.h*CRB1*, codon optimized AAV.h*CRB2*, AAV.*GFP* and *CRB1-B* were added using the known FASTA sequence.

Filtered expression matrices were further processed with a Seurat (v4.1.0) based workflow in in R (v4.1.0) [4]. In short, cells were demultiplexed based on their HTO enrichment using HTODemux function of Seurat, and singlets were selected for downstream analysis. Quality control followed, keeping cells with nFeature_RNA > 800 and <6000, nCount_RNA <30000, and percent.mt <12. The raw counts were normalized with NormalizedData function (scale.factor = 30000). The top 2000 most variable genes were selected using FindVariableFeatures. Principal component analysis (PCA) was then performed using these 2000 genes. The first 15 PCs were used to calculate cell clusters and project the cells on a two-dimensional plot using Uniform Manifold Approximation and Projection (UMAP) algorithm. Top markers from FindAllMarkers function were analysed and compared to well-known cell type-specific markers to classify the clusters. For downstream analysis, data was subset per cluster, per patient derived retinal organoids, and/or per treatment. Then, differentially expressed genes were retrieved from the FindMarkers function. Genes with p_val_adj ≤ 0,05 were used for GO (Gene Ontology) term analysis, GO analysis was performed using g:Profiler (version e106_eg53_p16_65fcd97) with g:SCS multiple testing correction method applying significance threshold of 0.05 [5]. Relevant terms and associated genes were included for visualization in this manuscript. For the violin plots comparing genes in CRB1 patient-derived and isogenic control retinal organoids, the function stat_compare_means with a Wilcoxon t-test was used to determine statistically significant differences.

Number of cells used for downstream analysis per condition: (1) coming from one sequencing round, ISO-P116 with AAV.*GFP*: *n*=993 cells from 4 organoids, P116 with AAV.*GFP*: *n*=1497 cells from 4 organoids, P116 with AAV.h*CRB1* and AAV.*GFP*: *n*=1225 cells from 3 organoids, P116 with AAV.h*CRB2* and AAV.*GFP*: *n* = 884 cells

from 3 organoids, and (2) equally divided in three separate sequencing rounds, ISO-P128 with AAV.*GFP*: n = 5786 cells from 6 organoids, P128 with AAV.*GFP*: n = 4908 cells from 6 organoids, P128 with AAV.h*CRB1* and AAV.*GFP*: n = 4386 cells from 5 organoids, P128 with AAV.h*CRB2* and AAV.*GFP*: n = 3870 cells from 5 organoids, P117 with AAV.*GFP*: n = 3552 cells from 5 organoids, P117 with AAV.h*CRB1* and AAV.*GFP*: n = 3108 cells from 5 organoids, P117 with AAV.h*CRB2* and AAV.*GFP*: n = 2868 cells from 5 organoids.

Supplemental references

1.   Quinn, P.M.; Buck, T.M.; Mulder, A.A.; Ohonin, C.; Alves, C.H.; Vos, R.M.; Bialecka, M.; van Herwaarden, T.; van Dijk, E.H.C.; Talib, M.; et al. Human iPSC-Derived Retinas Recapitulate the Fetal CRB1 CRB2 Complex Formation and Demonstrate that Photoreceptors and Müller Glia Are Targets of AAV5. *Stem Cell Reports* **2019**, *12*, 906–919, doi:10.1016/j.stemcr.2019.03.002.

2.   Zhong, X.; Gutierrez, C.; Xue, T.; Hampton, C.; Vergara, M.N.; Cao, L.H.; Peters, A.; Park, T.S.; Zambidis, E.T.; Meyer, J.S.; et al. Generation of three-dimensional retinal tissue with functional photoreceptors from human iPSCs. *Nat. Commun.* **2014**, *5*, doi:10.1038/ncomms5047.

3.   Pellissier, L.P.; Lundvig, D.M.S.; Tanimoto, N.; Klooster, J.; Vos, R.M.; Richard, F.; Sothilingam, V.; Garrido, M.G.; Bivic, A. Le; Seeliger, M.W.; et al. CRB2 acts as a modifying factor of CRB1-related retinal dystrophies in mice. *Hum. Mol. Genet*. **2014**, *23*, 3759–3771, doi:10.1093/hmg/ddu089.

4.   Hao, Y.; Hao, S.; Andersen-Nissen, E.; Mauck, W.M.; Zheng, S.; Butler, A.; Lee, M.J.; Wilk, A.J.; Darby, C.; Zager, M.; et al. Integrated analysis of multimodal single-cell data. *Cell* **2021**, *184*, 3573-3587.e29, doi:10.1016/j.cell.2021.04.048.

5.   Raudvere, U.; Kolberg, L.; Kuzmin, I.; Arak, T.; Adler, P.; Peterson, H.; Vilo, J. G:Profiler: A web server for functional enrichment analysis and conversions of gene lists (2019 update). *Nucleic Acids Res.* **2019**, *47*, W191–W198, doi:10.1093/nar/gkz369.

6.   Boon, N.; X. Lu, C. A. Andriessen, I. Moustakas, T. M. Buck, C. Freund, C. H. Arendzen, S. Böhringer, H. Mei, J. Wijnholds. AAV-mediated gene augmentation therapy of *CRB1* patient-derived retinal organoids restores the histological and transcriptional retinal phenotype. *Stem Cell Reports* **2023**

4